Constraining decaying dark matter with BOSS data and the effective field theory of large-scale structures

Théo Simon[1,*] Guillermo Franco Abellán,[1] Peizhi Du,[2] Vivian Poulin,[1] and Yuhsin Tsai[3]

[1]*Laboratoire Univers & Particules de Montpellier (LUPM), CNRS & Université de Montpellier (UMR-5299),*
Place Eugène Bataillon, F-34095 Montpellier Cedex 05, France
[2]*C.N. Yang Institute for Theoretical Physics, Stony Brook University, Stony Brook, New York 11794, USA*
[3]*Department of Physics, University of Notre Dame, Indiana 46556, USA*

We update cosmological constraints on two decaying dark matter models in light of BOSS-DR12 data analyzed under the effective field theory of large-scale structures (EFTofLSS) formalism, together with *Planck*, Pantheon and other BOSS measurements of the baryonic acoustic oscillation (BAO). In the first model, a fraction $f_{\rm dcdm}$ of cold dark matter (CDM) decays into dark radiation (DR) with a lifetime τ. In the second model (recently suggested as a potential resolution to the S_8 tension), all the CDM decays with a lifetime τ into DR and a massive warm dark matter (WDM) particle, with a fraction ε of the CDM rest mass energy transferred to the DR. Using numerical codes from the recent literature, we perform the first calculation of the mildly nonlinear (matter and galaxy) power spectra with the EFTofLSS for these two models. In the case of DR products, we obtain the constraints $f_{\rm dcdm} \lesssim 0.022$ (95% C.L.) for lifetimes shorter than the age of the Universe, and $\tau/f_{\rm dcdm} \gtrsim 250$ Gyr in the long-lived regime assuming $f_{\rm dcdm} \to 1$. We show that *Planck* data contributes the most to these constraints, with EFTofBOSS providing a marginal improvement over conventional BAO and redshift space distortions ($f\sigma_8$) data. In the case of DR and WDM decay products, we find that EFTofBOSS data significantly improves the constraints at 68% C.L. on the CDM lifetime with a S_8 prior from KiDS-1000. We show that, in order to fit EFTofBOSS data while lowering S_8 to match KiDS-1000, the best-fit model has a longer lifetime $\tau = 120$ Gyr, with a larger kick velocity $v_{\rm kick}/c \simeq \varepsilon \simeq 1.2\%$, than that without EFTofBOSS ($\tau = 43$ Gyr, $\varepsilon = 0.6\%$). We anticipate that future surveys will provide exquisite constraints on such models.

I. INTRODUCTION

The Λ cold dark matter (ΛCDM) model provides outstanding explanation for a wide variety of early universe data, such as cosmic microwave background (CMB) and big bang nucleosynthesis (BBN), as well as late universe observations of large scale structure (LSS) including the baryon acoustic oscillation (BAO), and uncalibrated luminosity distance to supernovae of type Ia (SNIa). Despite this remarkable success, the ΛCDM model does not teach us about the intrinsic nature of its dark sector, made up of both cold dark matter (CDM) and dark energy (DE). In addition, as the accuracy of cosmological observations has improved, the concordance cosmological model starts showing several experimental discrepancies. The most famous and important cosmological puzzle, the so-called Hubble tension [1], corresponds to a large discrepancy (~ 4–5σ) between the local determination of H_0 from a variety of methods—and in particular the cosmic distance ladder based on cepheid-calibrated SNIa by the SH0ES

team [2]—and its determination using CMB data under the assumption that the Universe is described by the ΛCDM model [3]. Another intriguing cosmological conundrum, the one at the heart of this study, is a less significant but older tension (~ 2–3σ) between the weak lensing[1] [6–9] and CMB [3,10] determinations of the amplitude of the local matter fluctuations, parametrized as $S_8 = \sigma_8\sqrt{\Omega_m/0.3}$, where Ω_m is the current total matter abundance, and σ_8 corresponds to the root mean square of matter fluctuations on a $8h^{-1}$ Mpc scale, with $h = H_0/(100\ {\rm km/s/Mpc})$, and is defined as follows:

$$\sigma_8^2 = \int \frac{k^3}{2\pi^2} P_m(k) W_8^2(k) d\ln k. \tag{1}$$

Here $P_m(k)$ is the linear matter power spectrum, and $W_8(k)$ is a window function describing a sphere (in Fourier space) with a (historically chosen) radius of $8h^{-1}$ Mpc.

---

[1]More precisely, there even exists a "lensing is low" anomaly when comparing galaxy clustering and weak lensing data within the ΛCDM cosmology [4–6].

*theo.simon@umontpellier.fr

Barring unknown systematic errors (see e.g., [2,6,11] for discussion), these discrepancies might be the first clue about the intrinsic nature of the ΛCDM dark sector. On the one hand, the resolution of the Hubble tension most likely involves new physics in the pre-recombination era,[2] through a decrease of the sound horizon before recombination [14–19], such as a model involving dark radiation and/or new neutrino properties [20–29], early dark energy [30–35], modified gravity [36–55] or exotic recombination [56–60] (for review, see Refs. [19,61]). On the other hand, the resolution of the S_8 tension requires a suppression in the matter power spectrum for $k \sim 0.1$–$1h$ Mpc^{-1} in order to reduce the value of the σ_8 parameter [see Eq. (1)], which can be achieved through a number of models that take into account new hypothetical properties of dark matter (DM) and/or DE [60,62–72].

Decaying cold dark matter (DCDM) models, in which dark matter is unstable on a cosmological timescale and decays into invisible products, have been proposed as potential resolutions to cosmic tensions [70,73–77]. In the past it was found that DM models with purely radiation decay products can neither resolve the Hubble tension nor the S_8 tension [78–84], while DM models with massive decay products can resolve the S_8 tension, as the massive particle produced during the decay acts as a WDM component, reducing power on scale below the free-streaming length at late times [70,77]. Beyond recent observational tensions, the study of these models is important from the particle physics point of view, as it addresses the question of the stability of DM on long cosmological timescales. In the literature, there are many models involving the existence of DM decays at late times, such as models with R-parity violation [85,86], super weakly interacting massive particles [87–90], sterile neutrinos [91,92], models with an additional U(1) gauge symmetry [93–96], or more recently a model of decaying warm dark matter [97]. Besides cosmic tensions, some DCDM models were proposed as a way to explain the excess of events in the electronic recoils reported by the Xenon1T collaboration [70,77,98–100]. In addition, DCDM models with massive daughters have also been suggested as a potential solution to the small (subgalactic) scales structure problem of CDM (e.g., [95,101–108]).

In this article, we deal with DCDM with two types of decay products: (i) the DCDM → DR model, where the decay products is only composed of a (massless) dark radiation (DR) component, and (ii) the DCDM → WDM + DR model, where the decay products are one massive WDM component and one DR component. Previous works have limited themselves to the impact of DCDM decay at

the background and linear perturbations level, deriving constraints (and hints) on these models from a combination of *Planck* CMB, BAO and uncalibrated luminosity distance to SN1a data. Here, we go beyond previous works by making use of the effective field theory of large scale structures (EFTofLSS) to describe the mildly nonlinear regime of the galaxy clustering power spectrum and derive improved constraints thanks to the EFTofLSS applied to BOSS data. The main objectives of this paper are: (i) perform the first-ever computation of the mildly nonlinear regime in DCDM models with massive and massless decay products through the EFTofLSS; (ii) test whether current BOSS data can lead to stronger constraints on these models; and (iii) check whether these constraints can put pressure on DCDM models that resolve the S_8 tension.

Our paper is structured as follows: in Sec. II, we briefly review the EFTofLSS formalism, the observable at hand and the public codes available to perform our analyses; in Sec. III, we introduce the models and present the nonlinear power spectrum computed with the EFTofLSS; in Sec. IV, we present the results of comprehensive Monte Carlo Markov chain (MCMC) analyses of the DCDM model and discuss the implications of these constraints for the S_8 tension; we eventually conclude in Sec. V. Appendix A is dedicated to comparing results of the EFTofLSS with N-body simulations in the DCDM → DR model, while Appendix B details the scope of our computation in the DCDM → WDM + DR model. Finally Appendixes C, D and E present additional results of the MCMC analyses for completeness.

II. THE GALAXY POWER SPECTRUM FROM THE EFTofLSS FORMALISM

Although an exhaustive review of the EFTofLSS is beyond the scope of this paper,[3] in this section, we briefly discuss the software tools that are available in the literature making use of the EFTofLSS to analyze the full shape of the galaxy clustering power spectrum as measured by BOSS. The relevant observables are the multipoles of the galaxy power spectrum, which are obtained through Legendre polynomials ($\mathcal{L}_l$) decomposition:

$$P_l(z, k) = \frac{2l+1}{2} \int_{-1}^{1} d\mu \mathcal{L}_l(\mu) P_{gg}(z, k, \mu), \qquad (2)$$

where z is the redshift, $\mu = \hat{z} \cdot \hat{k}$ is the angle between the line-of-sight z and the wave vector of the Fourier mode $\boldsymbol{k}$,

---

[2]We note that recent analysis based on the equality scale k_{eq} seems to disfavor some of the most extreme models suggested to resolve the tension and could eventually provide a challenge to early-universe models [12,13].

[3]The first formulation of the EFTofLSS was carried out in Eulerian space in Refs. [109,110] and in Lagrangian space in [111]. Once this theoretical framework was established, many efforts were made to improve this theory and make it predictive, such as the understanding of renormalization [112,113], the IR resummation of the long displacement fields [114–119], and the computation of the two-loop power spectrum [120,121]. Then, this theory was developed in the framework of biased tracers (such as galaxies and halos) in Refs. [122–127].

and $P_{gg}(z, k, \mu)$ is the redshift-space (nonlinear) galaxy power spectrum at one-loop order (see the appendix of Ref. [128] for the formal expression). This expression includes the "Alcock-Paczynski transformation" which takes into account the fact that the observation uses artificial cosmological parameters to convert redshifts as well as celestial coordinates into Cartesian coordinates. The two main contributions to $P_{gg}(z, k, \mu)$ are the monopole ($l = 0$) and the quadrupole ($l = 2$). Currently, there are two codes in the literature that model nonlinear effects on the power spectrum at one loop [including a proper infrared resummation (IR) [114–119] and a number of observational systematics corrections beyond the Alcock-Paczynski effect [129], such as window functions [130] and fiber collisions [131]] through the EFTofLSS method and which allows us to determine the monopole and the quadrupole of the galaxy power spectrum: (i) the PyBird[4] code [128]—a python module that determines the nonlinear matter power spectrum from the linear one returned by a Boltzmann code such as CLASS[5] [132] or CAMB[6] [133], and (ii) the CLASS-PT[7] code [134]—which is a stand-alone extension of the CLASS code. Both codes take into account the same effects with respect to a standard linear Boltzmann code, and in particular make use of the "FFTLog method" [135,136] to compute the one-loop power spectrum and the IR resummation. Given that our $\text{DCDM} \rightarrow \text{WDM} + \text{DR}$ study makes use of an independent extension to the CLASS code, we will rely on the PyBird code. We provide a comparison between the two codes in the context of the $\text{DCDM} \rightarrow \text{DR}$ model (already implemented in CLASS-PT) in Appendix A. One might wonder whether the EFTofLSS formalism must be extended to properly described the models under consideration. In Appendixes A and B, we argue that the current formalism (and the codes in their standard form) is sufficient to describe the DCDM models given present constraints and precision of the data. Yet, we anticipate that the formalism will need to be developed further for future surveys such as Euclid [137] and the LSST/Vera Rubin Observatory (VRO) [138], which will reach subpercent precision.

The data we use, in order to confront the nonlinear galaxy power spectrum forecasts with the observations, are made of three different sky-cuts from BOSS DR12 [139–141]: LOWZ NGC, CMASS NGC and CMASS SGC. LOWZ corresponds to the BOSS DR12 data including the BAO postreconstruction for $0.2 < z < 0.43$ and has an effective redshift $z_{\text{eff,LOWZ}} = 0.32$, while CMASS corresponds to the BOSS DR12 data also including the BAO postreconstruction for $0.43 < z < 0.7$ and has an effective redshift $z_{\text{eff,CMASS}} = 0.57$ (see Ref. [142]). This dataset will

be called, in the following, "EFTofBOSS data." Finally, it is worth noting that the EFTofLSS method has been tested against various simulations ([128,143–145]), and it has been highlighted that the BOSS full shape can only be evaluated up to $k_{\text{max}} \sim 0.2h \text{ Mpc}^{-1}$, where the BOSS full shape corresponds to the combination of the monopoles and quadrupoles of the power spectra of LOWZ NGC, CMASS NGC and CMASS SGC. To be more precise, we consider that $k_{\text{max,LOWZ}} = 0.2h \text{ Mpc}^{-1}$ and $k_{\text{max,CMASS}} = 0.23h \text{ Mpc}^{-1}$. Finally, we mention that the PyBird code makes use of ten additional nuisance parameters per sky-cut to describe various aspects of the EFTofLSS (for more details see e.g., [126]):

  (i)   four parameters b_i ($i = 1, 2, 3, 4$) to describe the galaxy bias at one-loop order;
 (ii)   three parameters c_{ct}, $c_{r,1}$, and $c_{r,2}$ corresponding to counterterms. c_{ct} is a linear combination of a higher derivative bias and the dark matter sound speed, while $c_{r,1}$ and $c_{r,2}$ are the redshift-space counterterms;
(iii)   three parameters $c_{\epsilon,0}$, $c_{\epsilon,1}$ and $c_{\epsilon,2}$ which describe stochastic contributions.

In practice, we make use of the analytical marginalization of Ref. [146] (Appendix C)[8] such that only two extra parameters per sky-cut are required in the analysis.

III. NONLINEAR POWER SPECTRUM IN DCDM COSMOLOGIES

In this section, we review the models of decaying dark matter considered in this work, and present the first computation of the nonlinear power spectra in these cosmologies. We consider two different DCDM models (both are limited to decay into the dark sector): one in which a fraction of dark matter decays into massless particles, and the second one in which all of the dark matter experiences two-body decay into massive and massless particles.

A. Dark radiation decay products ($\text{DCDM} \rightarrow \text{DR}$ model)

1. Presentation of the model

In the first model we consider, the cold DM sector is partially composed of an unstable particle (denoted as DCDM) that decays into a noninteracting relativistic particle (denoted as DR). The rest of the DM is considered stable and we refer to it as the standard CDM. In addition to the standard six ΛCDM parameters, there are two free parameters describing the lifetime of DCDM τ (or

---

[4]https://github.com/pierrexyz/pybird.
[5]https://lesgourg.github.io/class_public/class.html.
[6]https://camb.info/.
[7]https://github.com/Michalychforever/CLASS-PT.

[8]When discussing best fits however, we also optimize the nuisance parameters that are analytically marginalized in the MCMC.

equivalently the decay width $\Gamma = \tau^{-1}$), as well as the fraction of DCDM to total dark matter at the initial time $a_{\mathrm{ini}} \to 0$:

$$f_{\mathrm{dcdm}} \equiv \frac{\omega_{\mathrm{dcdm}}(a_{\mathrm{ini}})}{\omega_{\mathrm{tot,dm}}(a_{\mathrm{ini}})}, \qquad (3)$$

with $\omega_{\mathrm{tot,dm}} \equiv \omega_{\mathrm{dcdm}} + \omega_{\mathrm{cdm}}$. With these definitions, in the limit of large τ and/or small f_{dcdm}, one recovers the ΛCDM model.

The evolution of the homogeneous energy densities of the decaying dark matter and dark radiation is given by (see e.g., Refs. [80,147,148])

$$\dot{\bar{\rho}}_{\mathrm{dcdm}} + 3\mathcal{H}\bar{\rho}_{\mathrm{dcdm}} = -a\Gamma\bar{\rho}_{\mathrm{dcdm}}, \qquad (4)$$

$$\dot{\bar{\rho}}_{\mathrm{dr}} + 4\mathcal{H}\bar{\rho}_{\mathrm{dr}} = a\Gamma\bar{\rho}_{\mathrm{dcdm}}, \qquad (5)$$

where $\mathcal{H}$ is the conformal Hubble parameter,

$$\mathcal{H}^2(a) = \frac{8\pi G a^2}{3}\sum_i \bar{\rho}_i(a), \qquad (6)$$

with

$$\sum_i \bar{\rho}_i(a) = \bar{\rho}_{\mathrm{cdm}}(a) + \bar{\rho}_{\mathrm{dcdm}}(a) + \bar{\rho}_{\mathrm{dr}}(a)$$
$$+ \bar{\rho}_\gamma(a) + \bar{\rho}_\nu(a) + \bar{\rho}_b(a) + \bar{\rho}_\Lambda. \qquad (7)$$

To describe the evolution of the linearly perturbed universe, we consider the usual synchronous gauge, where the scalar part of the perturbed metric is written as [149]

$$ds^2 = a^2(\tau)[-d\tau^2 + (\delta_{ij} + h_{ij}(\boldsymbol{x}, t))dx^i dx^j]. \qquad (8)$$

Here τ is the conformal time, and $h_{ij}(\boldsymbol{x}, \tau)$ is defined as

$$h_{ij}(\boldsymbol{x}, \tau) = \int d^3 k e^{i\boldsymbol{k}\cdot\boldsymbol{x}}\left[\hat{k}_i\hat{k}_j h(\boldsymbol{k}, \tau)\right.$$
$$\left. + \left(\hat{k}_i\hat{k}_j - \frac{1}{3}\delta_{ij}\right)6\eta(\boldsymbol{k}, \tau)\right]. \qquad (9)$$

h denotes the trace of h_{ij}, while η corresponds to the other traceless scalar degree of freedom of the metric perturbation in Fourier space. Additionally, we consider the frame comoving with the DCDM (and CDM) fluid, such that $\theta_{\mathrm{dcdm}} = \partial_i v^i_{\mathrm{dcdm}} = 0$, where θ_{dcdm} is the divergence of the DCDM velocity v^i_{dcdm}. As a result, the energy density perturbation of the DCDM component, $\delta_{\mathrm{dcdm}} \equiv \rho_{\mathrm{dcdm}}/\bar{\rho}_{\mathrm{dcdm}} - 1$, follows the same evolution as standard CDM:

$$\dot{\delta}_{\mathrm{dcdm}} = -\frac{\dot{h}}{2}. \qquad (10)$$

The evolution of the linear perturbations of the DR integrated phase-space distribution multipoles is governed by the following hierarchy of equations [80,147,148]:

$$\dot{F}_{\mathrm{dr},0} = -kF_{\mathrm{dr},1} - \frac{2}{3}r_{\mathrm{dr}}\dot{h} + \dot{r}_{\mathrm{dr}}\delta_{\mathrm{dcdm}}, \qquad (11)$$

$$\dot{F}_{\mathrm{dr},1} = \frac{k}{3}F_{\mathrm{dr},0} - \frac{2k}{3}F_{\mathrm{dr},2}, \qquad (12)$$

$$\dot{F}_{\mathrm{dr},2} = \frac{2k}{5}F_{\mathrm{dr},1} - \frac{3k}{5}F_{\mathrm{dr},3} + \frac{4}{15}r_{\mathrm{dr}}(\dot{h} + 6\dot{\eta}), \qquad (13)$$

$$\dot{F}_{\mathrm{dr},\ell} = \frac{k}{(2\ell+1)}[\ell F_{\mathrm{dr},\ell-1} - (\ell+1)F_{\mathrm{dr},\ell+1}] \quad (\ell \geq 3). \qquad (14)$$

In the previous equations we have introduced $r_{\mathrm{dr}} \equiv a^4\bar{\rho}_{\mathrm{dr}}(a)/\rho_{c,0}$ following Ref. [80], where $\rho_{c,0}$ is the critical density today. In the scenario under study, we have

$$\dot{r}_{\mathrm{dr}} = a\Gamma(\bar{\rho}_{\mathrm{dcdm}}/\bar{\rho}_{\mathrm{dr}})r_{\mathrm{dr}}. \qquad (15)$$

We also note that the first three multipoles are simply related to elements of the perturbed stress-energy tensor as $F_{\mathrm{dr},0} = r_{\mathrm{dr}}\delta_{\mathrm{dr}}$, $F_{\mathrm{dr},1} = (4r_{\mathrm{dr}}/3k)\theta_{\mathrm{dr}}$, and $F_{\mathrm{dr},2} = 2\sigma_{\mathrm{dr}}r_{\mathrm{dr}}$. In order to truncate the hierarchy of Eqs. (11)–(14) at some $\ell_{\max} = 17$, we adopt the scheme proposed in Ref. [149] for massless neutrinos (and extended in CLASS to include nonzero curvature [150]) in order to limit the propagation of the error from $\ell_{\max}$ to ℓ. We extrapolate the behavior of $F_{\mathrm{dr},\ell_{\max}+1}$ thanks to the recursion relation:

$$F_{\mathrm{dr},\ell_{\max}+1} \approx \frac{2\ell_{\max}+1}{k\tau}F_{\mathrm{dr},\ell_{\max}} - F_{\mathrm{dr},\ell_{\max}-1}. \qquad (16)$$

These equations have been implemented in the Boltzmann code CLASS, and the impact of DCDM $\to$ DR decay on the (linear) CMB and matter power spectrum has been studied in detail in the literature [80,147,148]. In Appendix A we present a comparison of the EFTofLSS calculation with N-body simulations performed in Ref. [151]. The results obtained from these two methods agree up to subpercent difference for $k \lesssim 0.2h\ \mathrm{Mpc}^{-1}$ and $z = 0$, justifying that one can safely analyze the (mildly) nonlinear galaxy power spectrum with the EFTofLSS.

2. The nonlinear power spectrum

Thanks to the PyBird code, we plot in Fig. 1 the residuals of the nonlinear matter power spectra of the DCDM $\to$ DR model with respect to that of the ΛCDM model at $z = 0$.
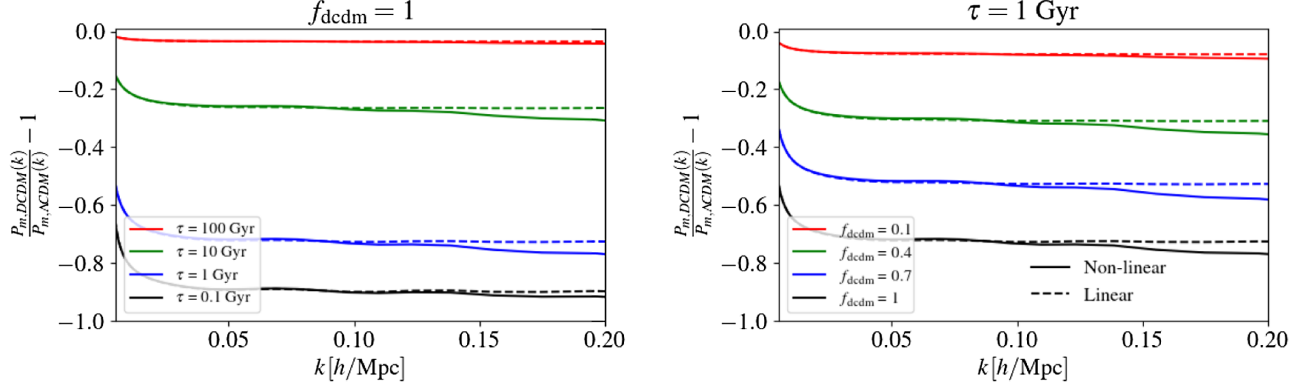
FIG. 1. Left: residuals of the linear (dashed lines) and nonlinear matter power spectrum (solid lines) for f_{dcdm} set to 1 and $\tau = 0.1$, 1, 10, 100 Gyr. Residuals are taken with respect to the ΛCDM model at $z = 0$. Right: the same, but this time τ is set to 1 Gyr and $f_{dcdm} = 0.1, 0.4, 0.7, 1$.

We also represent the associated linear matter power spectra obtained from the CLASS code. In addition, we plot in Fig. 2 the residuals of the monopole and quadrupole of the galaxy power spectra of this model. In these figures, we set the ΛCDM parameters[9] to their best-fit values from the analysis of $Planck + \text{Pantheon} + \text{EFTofBOSS} + \text{Ext-BAO}$ (as described in Sec. IV). Finally, we simply vary the two parameters f_{dcdm} and τ to isolate their cosmological effects: in the left panels, we fix $f_{dcdm} = 1$ and vary $\tau \in [0.1, 1000]$ Gyr, while in the right panel we fix $\tau = 1$ Gyr and vary $f_{dcdm} \in [0.1, 1]$.

From Figs. 1 and 2, one can see that the monopole of the galaxy power spectrum shows a behavior very similar to that of the linear matter spectrum. For a realistic choice of EFT parameters, it shows an almost scale-independent power suppression due to two main reasons [80,147]. First, the decay of DCDM decreases the duration of the matter dominated era (and at fix h, a smaller Ω_m/larger Ω_Λ), implying a shift of the power spectrum towards large scales, i.e., towards small wave numbers. Second, DCDM models involve a larger ratio of ω_b/ω_{cdm} compared to the ΛCDM model due to the decay. Both effects manifest as a strong suppression of the small-scale power spectrum, and the latter effect leads to an additional modulation of the BAO amplitude visible as wiggles in Figs. 1 and 2. Moreover, we note that the nonlinear matter power spectrum shows a stronger scale-dependent suppression compared to the linear power spectrum at $k \gtrsim 0.1h$ Mpc^{-1}. There is an

intuitive explanation as to why the nonlinear power spectrum is further suppressed, very similarly to what happens for standard neutrinos or warm dark matter, as reviewed e.g., in [152]. In general, nonlinear growth is faster than the linear growth, and the impact of non-linearities is typically to enhance the power spectrum (this is famously the case in ΛCDM). In the DCDM case, modes that are suppressed will enter the nonlinear regime later, and therefore start experiencing their enhanced growth due to nonlinearities later. This delay leads to a further suppression of the power spectrum compared to ΛCDM when nonlinear effects are included. We checked that the amplitude of the deviation from scale-independent suppression at $k \gtrsim 0.1h$ Mpc^{-1} is tied to the value of the effective dark matter sound speed c_s, and can vary a few % for $c_s \in [1, 5]$ $k_{nl}^2 \cdot (\text{Mpc}/h)^2$, where k_{nl} corresponds to the nonlinear scale and determines the cutoff scale of the theory. On the other hand, the power suppression gets less strong with larger k in the monopole of the galaxy power spectrum, an effect indicating an additional degeneracy with other EFT parameters. Finally, and as expected, deviations with respect to ΛCDM increases as τ decreases and/or f_{dcdm} increases for the monopole as well as for the quadrupole.

3. Preliminary study

To gauge the impact of using the EFTofBOSS data in our analyses of the DCDM → DR model, we first perform a preliminary study in which we consider a set of DCDM parameters laying at the 95% C.L.[10] derived from $Planck$ data, and compute the χ^2 of the EFTofBOSS data after optimizing the EFT nuisance parameters. The goal is to check the extent to which EFT nuisance parameters can lead to effects degenerate with those of the DCDM with a quick analysis. We set all ΛCDM parameters to their

---

[9]For completeness, note that the shape of the residuals of the galaxy and matter power spectra depend on the values of the EFT nuisance parameters, especially at large k. According to the notation of Ref. [128], for the numerical evaluation we set the effective dark matter sound speed $c_s = 1$ for the matter power spectra, and $b_1 = 2$, $b_2 = 1$, $b_3 = 0.5$, $b_4 = 0$, $c_{ct} = 0.5$, $c_{r,1} = 2$ and $c_{r,2} = c_{\epsilon,0} = c_{\epsilon,1} = c_{\epsilon,2} = 0$ for the galaxy power spectra. In practice, these parameters are optimized when quoting best fits, to ensure that they take realistic values.

[10]From here on, we quote one-sided bounds at 2σ (95% C.L.) and two-sided bounds at 1σ (68% C.L.).
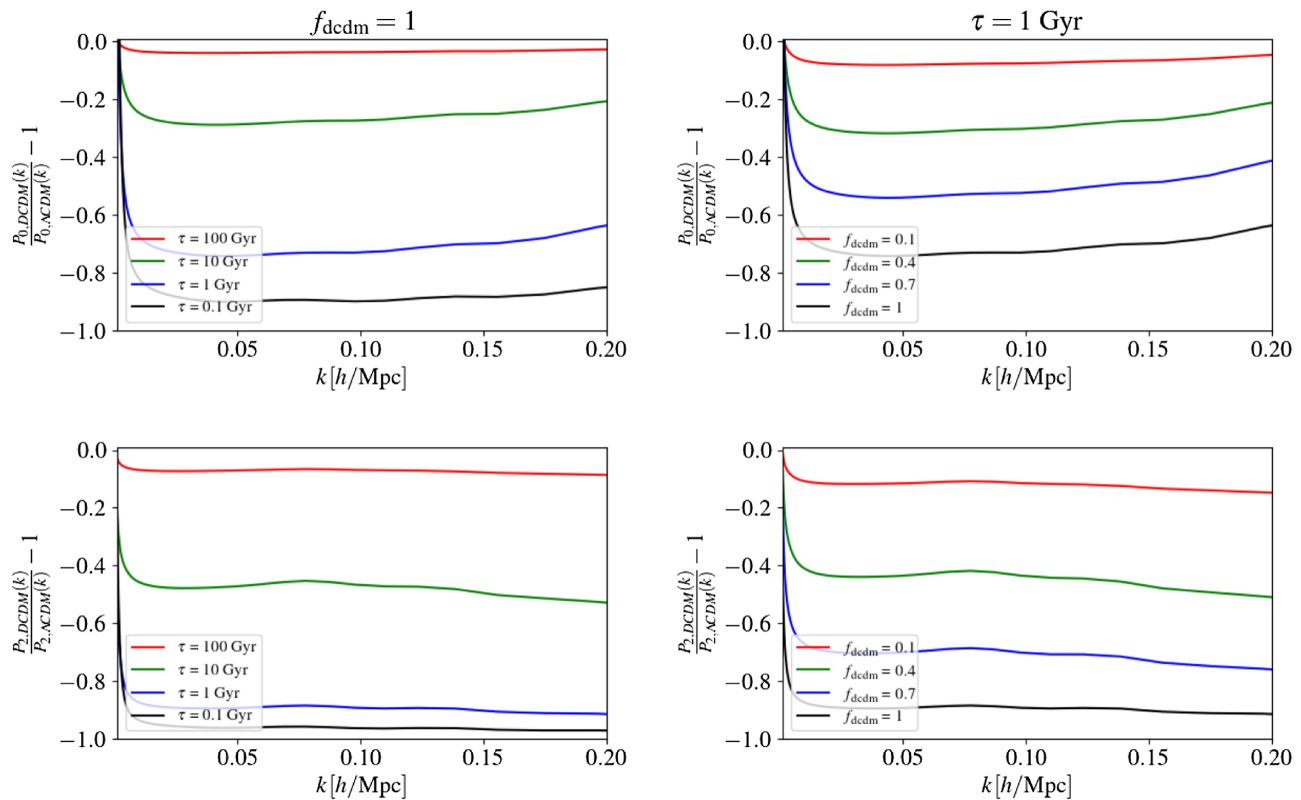
FIG. 2.   Left: residuals of the monopole and the quadrupole of the galaxy power spectrum for f_{dcdm} set to 1 and $\tau = 0.1, 1, 10, 100$ Gyr. Residuals are taken with respect to the ΛCDM model at $z = 0$. Right: the same, but this time τ is set to 1 Gyr and $f_{dcdm} = 0.1, 0.4, 0.7, 1$.

best-fit values from the analysis of $Planck$ + Pantheon + EFTofBOSS + Ext-BAO (see Sec. IV). We perform two analyses: (i) we set $\tau = 0.1$ Gyr and take the upper bound on f_{dcdm} from our $Planck$ + Pantheon + Ext-BAO (no Ly-α), i.e., $f_{dcdm} = 0.0203$ (see Table V), and (ii) we set $f_{dcdm} = 1$ (i.e., all the dark matter decays), while we take the lower bound of τ from our $Planck$ + Pantheon + Ext-BAO (no Ly-α) analysis, i.e., $\tau = 248.4$ Gyr (see Table V). We show in Table I the χ^2 associated to the EFTofBOSS data, and we plot in Fig. 3, using the PyBird code, the residuals (with respect to ΛCDM from the $Planck$ + Pantheon + EFTofBOSS + Ext-BAO analysis)

TABLE I. χ^2 of each sky-cut of the EFTofBOSS dataset for our DCDM → DR preliminary study. We also indicated the $\Delta\chi^2$ with respect to the analogous ΛCDM best-fit model (EFTofBOSS analysis in Table VII).

Parameter	$f_{dcdm} = 0.0203$ and $\tau = 0.1$ Gyr	$f_{dcdm} = 1$ and $\tau = 248.4$ Gyr
$\chi^2_{CMASS\ NGC}$	41.3	40.7
$\chi^2_{CMASS\ SGC}$	43.9	44.0
$\chi^2_{LOWZ\ NGC}$	33.4	33.6
$\chi^2_{EFTofBOSS}$	118.6	118.3
$\chi^2_{min}(DCDM) - \chi^2_{min}(\Lambda CDM)$	+0.8	+0.5

of these studies. To gauge the impact of EFT nuisance parameters, in this latter figure, we show residuals with and without the optimization procedure (in the latter case, we simply set the EFT nuisance parameters to those of ΛCDM). This preliminary study allows us to highlight two important points. First, the optimization procedure has washed out the suppression due to decay, which implies that the effect of the EFT nuisance parameters are (at least partly) degenerate with that of the decay. Second (and consequently), for these two analyses where we have chosen DCDM parameters that are excluded at 95% C.L., we obtain a χ^2 very close to that of the ΛCDM best-fit model of the full analysis, suggesting that EFTofBOSS data may not provide strong additional constraints to this model. Naturally, it does not prevent the model to potentially yield an improved fit over ΛCDM once all (cosmological and nuisance) parameters are optimized against the data, and we will check our naive results against a full analysis in Sec. IV.

B. Warm dark matter decay products (DCDM → WDM + DR model)

1. Presentation of the model

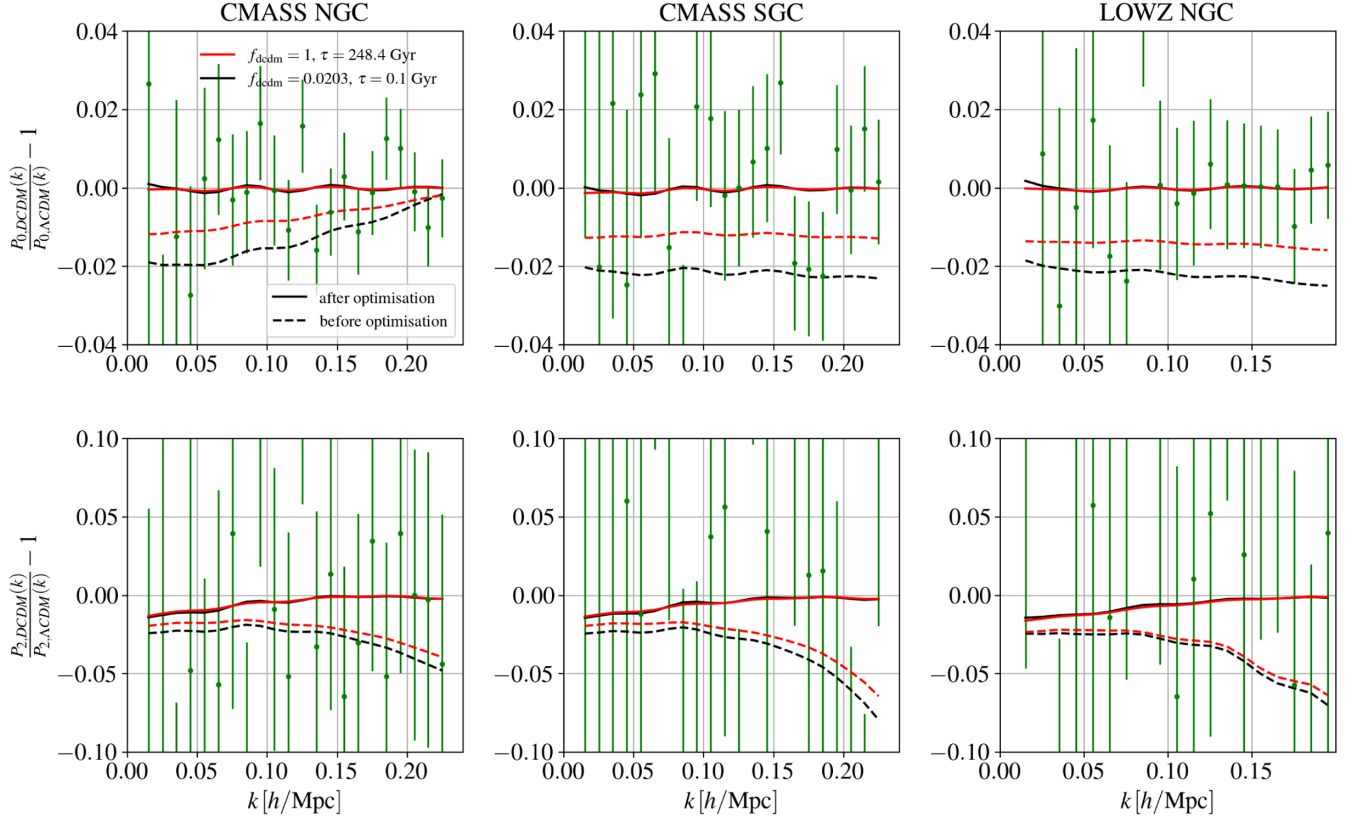We now turn to a DCDM model where the entirety of the DM sector is considered unstable (i.e., $f_{dcdm} = 1$ in the

FIG. 3. Residuals of the monopole and the quadrupole of our DCDM → DR preliminary study with respect to the ΛCDM model (EFTofBOSS analysis in Table III) for the three sky-cuts of the EFTofBOSS data. For the solid lines we optimized the EFT nuisance parameters, while for the dotted lines we set the EFT nuisance parameters to those of the ΛCDM (EFTofBOSS analysis in Table III).

language of the first model), decaying into dark radiation and a massive particle, which will act as WDM. As before, we assume the decay products do not interact with the standard model particles. The DCDM sector is now described by the DCDM lifetime τ, and the fraction ε of rest-mass energy carried away by the massless particle given by [153]

$$\varepsilon = \frac{1}{2}\left(1 - \frac{m_{\mathrm{wdm}}^2}{m_{\mathrm{dcdm}}^2}\right), \quad (17)$$

where m_{dcdm} and m_{wdm} are the mother and daughter particle masses respectively. The accurate computation of the cosmological impact of the DCDM sector requires to follow the evolution of the phase space distribution of the warm particle produced during the decay. The full set of equations is described in Refs. [77,154]. We summarize here the sets of equations describing the evolution of the background energy densities of the dark components, as well as the linear perturbations in a fluid approximation, valid well within the horizon.

The background energy densities evolve as follows [154]:

$$\dot{\bar{\rho}}_{\mathrm{dcdm}} + 3\mathcal{H}\bar{\rho}_{\mathrm{dcdm}} = -a\Gamma\bar{\rho}_{\mathrm{dcdm}}, \quad (18)$$

$$\dot{\bar{\rho}}_{\mathrm{wdm}} + 3(1+w)\mathcal{H}\bar{\rho}_{\mathrm{wdm}} = (1-\varepsilon)a\Gamma\bar{\rho}_{\mathrm{dcdm}}, \quad (19)$$

$$\dot{\bar{\rho}}_{\mathrm{dr}} + 4\mathcal{H}\bar{\rho}_{\mathrm{dr}} = \varepsilon\Gamma a\bar{\rho}_{\mathrm{dcdm}}, \quad (20)$$

where $w = \bar{P}_{\mathrm{wdm}}/\bar{\rho}_{\mathrm{wdm}}$ is the equation of state of the massive daughter particle. In the limit of large τ or small ε, one recovers the ΛCDM model, while setting $\varepsilon = 1/2$ leads to a decay solely into massless particles.

In the synchronous gauge comoving with the DCDM fluid, the linear perturbation equations for the parent particle and DR daughter is still given by Eq. (10) and Eqs. (11)–(14), respectively. However, the quantity r_{dr} now satisfies

$$\dot{r}_{\mathrm{dr}} = a\varepsilon\Gamma(\bar{\rho}_{\mathrm{dcdm}}/\bar{\rho}_{\mathrm{dr}})r_{\mathrm{dr}}, \quad (21)$$

where the parameter ε now affects the amount of energy transferred to the DR. Regarding the WDM linear perturbations, it is unfortunately not possible to integrate out the dependency on momenta as it is done for the DR species. In general one has to follow the evolution of the full phase-space distribution, which becomes very computationally demanding (see Ref. [77] for the expression of the full Boltzmann hierarchy). Nevertheless, it was shown in Ref. [77] that, well within the horizon, the dynamics of the WDM perturbations

can be well approximated by the following set of fluid equations:

$$\dot{\delta}_{\rm wdm} = -3\mathcal{H}(c_s^2 - \omega)\delta_{\rm wdm} - (1 + \omega)\left(\theta_{\rm wdm} + \frac{\dot{h}}{2}\right)$$

$$+ (1 - \varepsilon)a\Gamma\frac{\bar{\rho}_{\rm dcdm}}{\bar{\rho}_{\rm wdm}}(\delta_{\rm dcdm} - \delta_{\rm wdm}), \qquad (22)$$

$$\dot{\theta}_{\rm wdm} = -\mathcal{H}(1 - 3c_g^2)\theta_{\rm wdm} + \frac{c_s^2}{1 + \omega}k^2\delta_{\rm wdm} - k^2\sigma_{\rm wdm}$$

$$- (1 - \varepsilon)a\Gamma\frac{1 + c_g^2}{1 + \omega}\frac{\bar{\rho}_{\rm dcdm}}{\bar{\rho}_{\rm wdm}}\theta_{\rm wdm}, \qquad (23)$$

where c_s is the WDM sound speed in the synchronous gauge, i.e., $c_s^2 = \delta P_{\rm wdm}/\delta\rho_{\rm wdm}$, and c_g is the WDM adiabatic sound speed, i.e., $c_g^2 = \dot{\bar{P}}_{\rm wdm}/\dot{\bar{\rho}}_{\rm wdm}$, which one can write in the following form:

$$c_g^2 = w\left(5 - \frac{\mathfrak{p}_{\rm wdm}}{\bar{P}_{\rm wdm}} - \frac{\bar{\rho}_{\rm dcdm}}{\bar{\rho}_{\rm wdm}}\frac{a\Gamma}{3w\mathcal{H}}\frac{\varepsilon^2}{1 - \varepsilon}\right)$$

$$\times \left[3(1 + w) - \frac{\bar{\rho}_{\rm dcdm}}{\bar{\rho}_{\rm wdm}}\frac{a\Gamma}{\mathcal{H}}(1 - \varepsilon)\right]^{-1}. \qquad (24)$$

In this latter equation, $\mathfrak{p}_{\rm wdm}$ is the pseudo-pressure (introduced in the context of the fluid equations for massive neutrinos [155]), which corresponds to a higher momenta integral of the WDM homogeneous phase space distribution, reducing to the standard pressure in the relativistic limit. Solving the fluid equations requires specifying the sound speed c_s, which was found to be well described by the following formula:

$$c_s^2(k, \tau) = c_g^2[1 + 0.2 \times (1 - 2\varepsilon)\sqrt{k/k_{\rm fs}}], \qquad (25)$$

where the free-streaming scale $k_{\rm fs}$ of the WDM is computed as

$$k_{\rm fs}(\tau) = \sqrt{\frac{3}{2}}\frac{\mathcal{H}(\tau)}{c_g(\tau)}. \qquad (26)$$

The free-streaming scale corresponds to the scale at which pressure (coming from the "velocity kick" received during the decay process) suppresses perturbations of the WDM compared to those of the DCDM. In other words, on scales $k < k_{\rm fs}$, one has $\delta_{\rm wdm} = \delta_{\rm dcdm}$, while on scale $k > k_{\rm fs}$ the WDM perturbations are suppressed and exhibit oscillations over time.

To obtain the linear CMB and matter power spectrum, we make use of an extension of the CLASS code[11] described in Ref. [77], and we determine the nonlinear galaxy power spectrum using the PyBird code. We have argued in previous section and in Appendix A, through direct comparison with N-body simulations, that PyBird can

---

[11]https://github.com/PoulinV/class_decays

safely be used to describe DM decays with massless decay products. Unfortunately, we do not have access to such N-body simulations in the case of massive decay products. *A priori*, the problem is not the decay *per se* (as we have seen for the massless decay products). Rather, contrarily to the case of massless daughters, the massive daughter may develop perturbations whose contribution to the total matter power spectrum can be highly nontrivial. In Appendix B, following Refs [156,157], which treated the similar case of massive neutrinos, we argue that the corrections to the EFTofLSS necessary to fully capture the model-specific effects can be neglected for most of the parameter space of interest, as the fractional contribution of the WDM to the DM density is small (in particular for the best-fit model that we derive), or the free-streaming scale exceeds the scale cut considered in the analysis.

2. The nonlinear power spectrum

We plot in Fig. 4 the residuals of the nonlinear matter power spectra of the DCDM → WDM + DR model with respect to that of the ΛCDM model at $z = 0$. We also represent the associated linear matter power spectra obtained from the CLASS code, exactly as in Fig. 4 of Ref. [77]. In addition, we plot in Fig. 5 the residuals of the monopole and quadrupole of the galaxy power spectra of this model. In these figures, the cosmological parameters are taken from the DCDM → WDM + DR best-fit model of Ref. [70], while the nuisance parameters are set as in Figs. 1 and 2. In the left panels, we fix $\varepsilon = 0.1$ and vary $\tau \in [10, 300]$ Gyr, while in the right panel we fix $\tau = 30$ Gyr and vary $\varepsilon \in [0.001, 0.5]$.

As for the case of the DCDM → DR model, we obtain a very similar behavior between the linear matter power spectrum and the monopole of the galaxy power spectrum, except for a mild monotonic reduction of the power suppression at larger k's in the monopole of the galaxy power spectrum (due to the choice of EFT parameters, this reduction of the suppression may change for different values). The presence of a warm dark matter component which does not cluster on small scales suppresses the matter power spectrum as well as the galaxy power spectrum, and τ—which sets the abundance of the WDM species today—controls the amplitude of the power suppression, while ε controls the cutoff scale. One can see in Fig. 5 that the suppression of the galaxy spectrum increases as τ decreases (left panel), while the suppression starts to occur on larger scales as ε increases (right panel). Once $\varepsilon = 0.5$, the free-streaming scale $k_{\rm fs}$ becomes equivalent to the Hubble horizon, and the effects become identical to that of the DCDM → DR model presented before. Note that because of the effect of the WDM, the $\varepsilon = 0.1$ case has a stronger suppression than the $\varepsilon = 0.5$ (pure dark radiation) case. Moreover, we find (see Fig. 4) that the nonlinear correction slightly modulates the slope of the power suppression compared to the linear matter power spectrum. It always leads to a stronger suppression than the linear one at large enough k (for $\varepsilon \gtrsim 0.1$, the
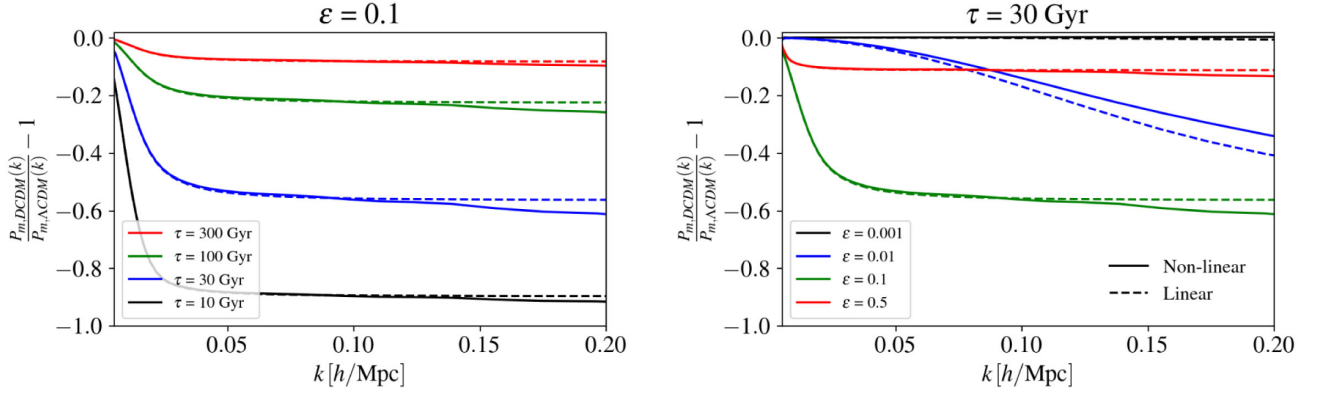
FIG. 4.   Left: residuals of the linear (dashed lines) and nonlinear matter power spectrum (solid lines) for ε set to 0.1 and $\tau = 10, 30, 100, 300$ Gyr. Residuals are taken with respect to the ΛCDM model at $z = 0$. Right: the same, but this time τ is set to 30 Gyr and $\varepsilon = 0.001, 0.01, 0.1, 0.5$.
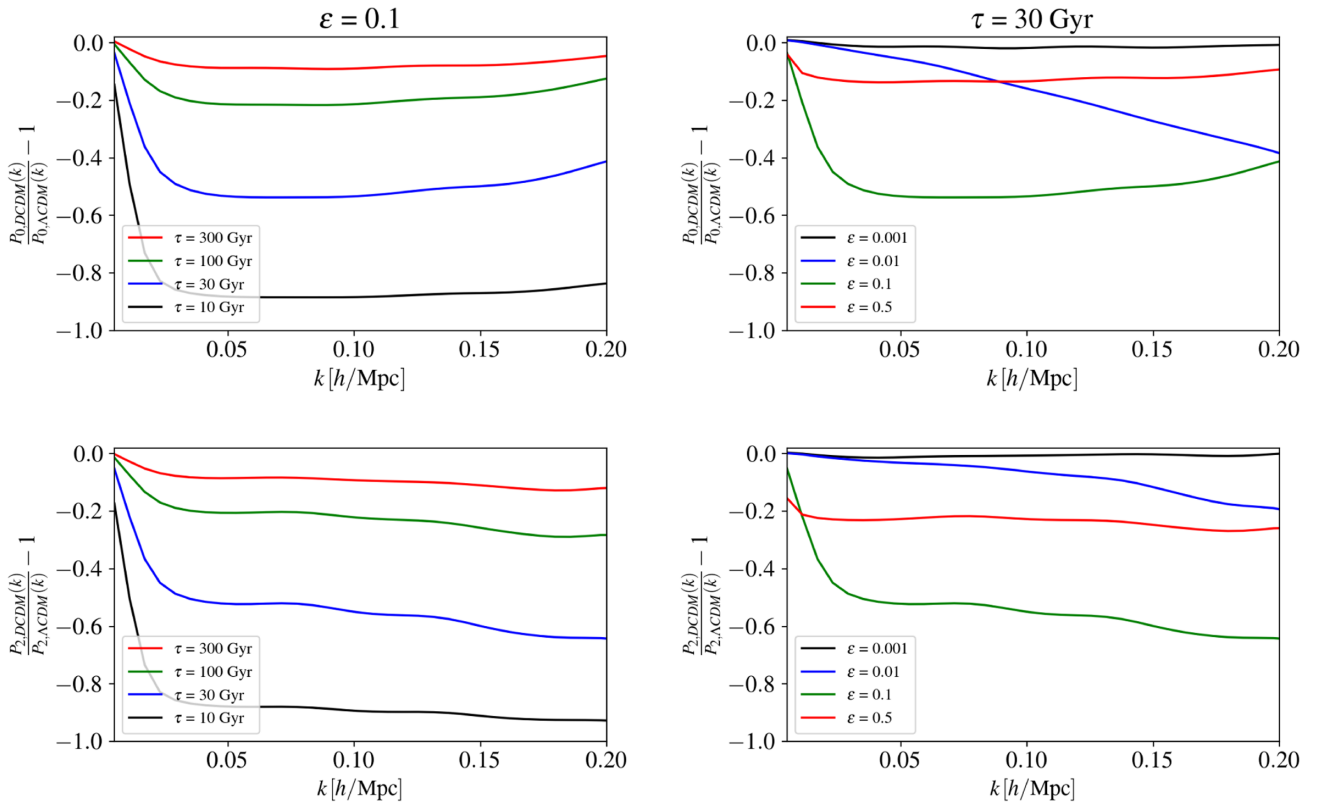

FIG. 5.   Left: residuals of the monopole and the quadrupole of the galaxy power spectrum for ε set to 0.1 and $\tau = 10, 30, 100, 300$ Gyr. Residuals are taken with respect to the ΛCDM model at $z = 0$. Right: the same, but this time τ is set to 30 Gyr and $\varepsilon = 0.001, 0.01, 0.1, 0.5$.

modulation occurs at $k \gtrsim 0.1h\ \mathrm{Mpc}^{-1}$). However, for smaller ε (see the $\varepsilon = 0.01$ case for example), the modulation can appear as a milder power suppression compared to the linear one in the range of validity of the EFT at one-loop order.

3. Preliminary study

Similarly to the case of the DCDM → DR model, we perform a preliminary study to test whether the

EFTofBOSS data can further constrain the DCDM → WDM + DR model that resolves the S_8 tension. We fix cosmological parameters[12] to those obtained from the

---

[12]The analysis performed in Refs. [70,77] made use of a S_8 prior that includes information from BOSS [158]. For consistency and to avoid double counting information, we reperformed the analysis (see Sec. IV) with a prior derived from KiDS-1000 data alone.

TABLE II. χ^2 of each sky-cut of the EFTofBOSS dataset for our DCDM $\rightarrow$ WDM + DR preliminary study. We also indicated the $\Delta\chi^2$ with respect to the analogous ΛCDM best-fit model (EFTofBOSS + S_8 analysis in Table VII).

Parameter	Best fit
$\chi^2_{\text{CMASS NGC}}$	41.2
$\chi^2_{\text{CMASS SGC}}$	44.5
$\chi^2_{\text{LOWZ NGC}}$	34.4
$\chi^2_{\text{EFTofBOSS}}$	120.1
$\chi^2_{\text{min}}(\text{DCDM}) - \chi^2_{\text{min}}(\Lambda\text{CDM})$	+3.1

joint analysis of *Planck* data, Pantheon SN1a data, a compilation of BAO data and the S_8 measurements by KiDS-1000 [7]. We optimize the EFT nuisance parameters of the galaxy power spectrum to check the extent to which they can lead to effects degenerate with those of the DCDM. We show in Table II the χ^2 associated to the EFTofBOSS data, while in Fig. 6, using the PyBird code, we plot the residuals with respect to the best-fit ΛCDM model from the analysis of *Planck* + Pantheon + EFTofBOSS + Ext-BAO (see Sec. IV). In this figure, we represent residuals with

and without the EFT optimization procedure (in the latter case, we simply set the EFT nuisance parameters to those of ΛCDM). As before, one can see that the effects of the DCDM are strongly reduced once EFT nuisance parameters are optimized, suggesting a strong degeneracy between the DCDM and the EFT parameters. Nevertheless, for this preliminary study, the χ^2 is degraded by +3.1 compared to the best-fit χ^2 obtained in the ΛCDM model for the full analysis. Contrary to the preliminary study of the DCDM $\rightarrow$ DR model for which we obtained a χ^2 close to that of the ΛCDM model, we anticipate that the EFTofBOSS data can provide additional constraining power to this model.

IV. A COMPREHENSIVE MCMC ANALYSIS OF THE DCDM MODELS

A. Data and method

We now perform a Monte Carlo Markov chain (MCMC) analyses, confronting these two DCDM models with recent cosmological observations. To do so, we make use of the MONTEPYTHON-v3 code [159,160] interfaced with our modified CLASS version. We perform various analyses from a combination of the following datasets:
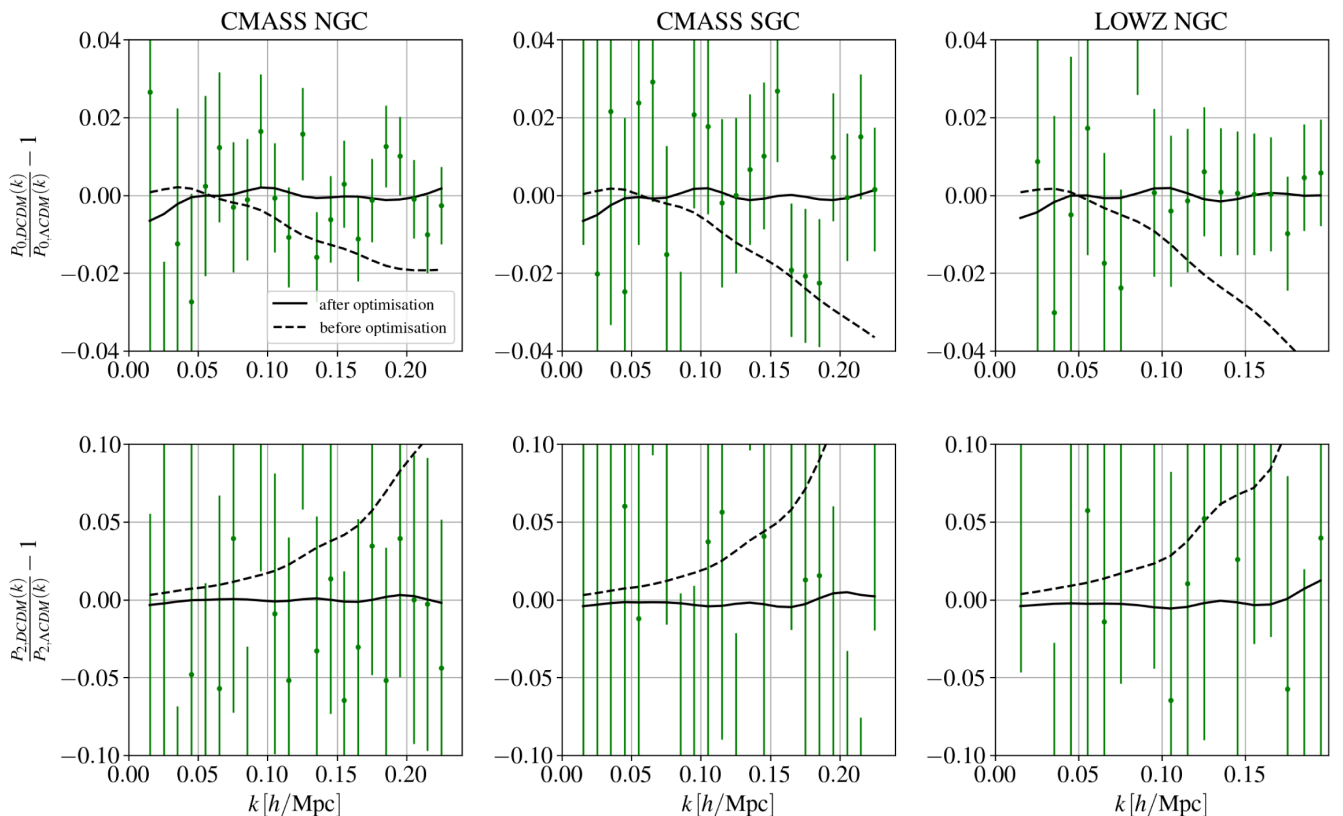

FIG. 6. Residuals of the monopole and the quadrupole of our DCDM $\rightarrow$ WDM + DR preliminary study with respect to ΛCDM model (EFTofBOSS analysis in Table III) for the three sky-cuts of the EFTofBOSS data. For the solid lines we optimized the EFT nuisance parameters, while for the dotted lines we set the EFT nuisance parameters to those of the ΛCDM (EFTofBOSS analysis in Table III).

TABLE III. The mean (best-fit) $\pm 1\sigma$ errors of the cosmological parameters from our $Planck$ + Pantheon + EFTofBOSS + Ext-BAO and $Planck$ + Pantheon + EFTofBOSS + Ext-BAO + S_8 analyses for the ΛCDM model. For each dataset we also report its best-fit χ^2.

	ΛCDM	
Parameter	w/EFTofBOSS	w/EFTofBOSS + S_8
$100\omega_{\mathrm{b}}$	$2.242(2.245)^{+0.014}_{-0.015}$	$2.247(2.248) \pm 0.014$
ω_{cdm}	$0.1191(0.1191) \pm 0.00095$	$0.1184(0.1184) \pm +0.00089$
$H_0/$ [km/s/Mpc]	$67.76(67.80)^{+0.42}_{-0.44}$	$68.05(68.07) \pm 0.41$
$\ln(10^{10}A_s)$	$3.048(3.049)^{+0.015}_{-0.016}$	$3.043(3.043)^{+0.015}_{-0.016}$
n_s	$0.9666(0.9676) \pm 0.0039$	$0.9680(0.9687) \pm 0.0039$
τ_{reio}	$0.0571(0.0574)^{+0.0075}_{-0.0085}$	$0.0555(0.0549)^{+0.0077}_{-0.0078}$
Ω_{m}	$0.3098(0.3093)^{+0.0057}_{-0.0058}$	$0.3057(0.3055) \pm 0.0053$
σ_8	$0.8097(0.8102)^{+0.0063}_{-0.0065}$	$0.8056(0.8055) \pm 0.0062$
S_8	$0.82(0.82) \pm 0.01$	$0.813(0.813)^{+0.0094}_{-0.0096}$
χ^2_{min}	3927.0	3933.0
$Q_{\mathrm{DMAP}} \equiv \sqrt{\chi^2_{\mathrm{min}}(\mathrm{w}/S_8) - \chi^2_{\mathrm{min}}(\mathrm{w/o}\,S_8)}$	2.4σ	

  (i) Planck: The low-l CMB TT, EE, and the high-l TT, TE, EE data, as well as the gravitational lensing potential reconstruction from $Planck$ 2018 [3,161].
 (ii) Pantheon: The Pantheon SNIa catalog, spanning redshifts $0.01 < z < 2.3$ [162].
(iii) Ext-BAO: The BAO measurements from 6dFGS at $z = 0.106$, SDSS DR7 at $z = 0.15$ [139,163,164], and the joint constraints from eBOSS DR14 Ly-α absorption autocorrelation at $z = 2.34$ and cross-correlation with quasars at $z = 2.35$ [165,166].
 (iv) BOSS BAO/$f\sigma_8$: The measurements of the BAO and the redshift space distortion $f\sigma_8(z)$ from the CMASS and LOWZ galaxy samples of BOSS DR12 at $z = 0.38$, 0.51, and 0.61 [139].
  (v) S_8: The KIDS-1000 cosmic shear measurement of $S_8 = 0.759^{+0.024}_{-0.021}$, modeled as a a split-normal likelihood [7].
 (vi) EFTofBOSS: The CMASS and LOWZ datasets of the EFTofBOSS data (see Sec. II).

Our analyses always includes $Planck$, Pantheon and Ext-BAO data. However, we quantify the impact of EFTofBOSS data and the S_8 prior by performing analyses with and without these data. When *not* including the EFTofBOSS data, we make use of the conventional BOSS BAO/$f\sigma_8$ data. We use $Planck$ conventions for the treatment of neutrinos and include two massless and one massive species with $m_\nu = 0.06$ eV [3]. We impose a large flat prior on the dimensionless baryon energy density ω_b, the Hubble parameter today H_0, the logarithm of the variance of curvature perturbations centered around the pivot scale $k_p = 0.05$ Mpc^{-1} (according to the $Planck$ convention), $\ln(10^{10}\mathcal{A}_s)$, the scalar spectral index n_s, and the reionization optical depth τ_{reio}. We assume our MCMC chains to be converged when the Gelman-Rubin

criterion $R - 1 < 0.05$ [167]. Finally, we extract the best-fit parameters from the procedure highlighted in the appendix of Ref. [19].

B. Dark radiation decay products

Let us recall that in the case of the DCDM → DR model we have two additional parameters: $\Gamma = \tau^{-1}$, the decay rate of DCDM, and f_{dcdm}, the fraction of DCDM with respect to the total DM. In the MCMC analyses, we impose flat priors on Γ and f:

$$0 \leq \Gamma/\mathrm{Gyr}^{-1} \leq 10,$$

$$0 \leq f_{\mathrm{dcdm}} \leq 1.$$

Our results for the analyses with and without S_8 prior are presented in Table IV, while the results of the analyses of ΛCDM against the same datasets are given in Table III. The χ^2 of the EFTofBOSS data are reported in Table VII. In Fig. 7, we display the 1D and 2D posteriors of $\{\Gamma/\mathrm{Gyr}^{-1}, f_{\mathrm{dcdm}}, H_0, S_8, \Omega_m\}$ for the DCDM → DR model with and without the EFTofBOSS dataset. In Appendix C, we represent the same figure, but this time with and without the S_8 prior (and with the EFTofBOSS dataset for both). Without the S_8 prior, the $\Delta\chi^2$ with respect to ΛCDM is compatible with zero[13] (see Table IV), implying that the data does not favor the DCDM → DR model. From Fig. 7, one can see that the inclusion of the EFTofBOSS data does not improve the constraint on this model,

---

[13]The improvement is below the precision of $\mathcal{O}(0.1)$ that we estimated on the minimization, and we therefore simply quote $\Delta\chi^2 = 0.0$. Hereafter, we follow the same approach when reporting other $\Delta\chi^2$.
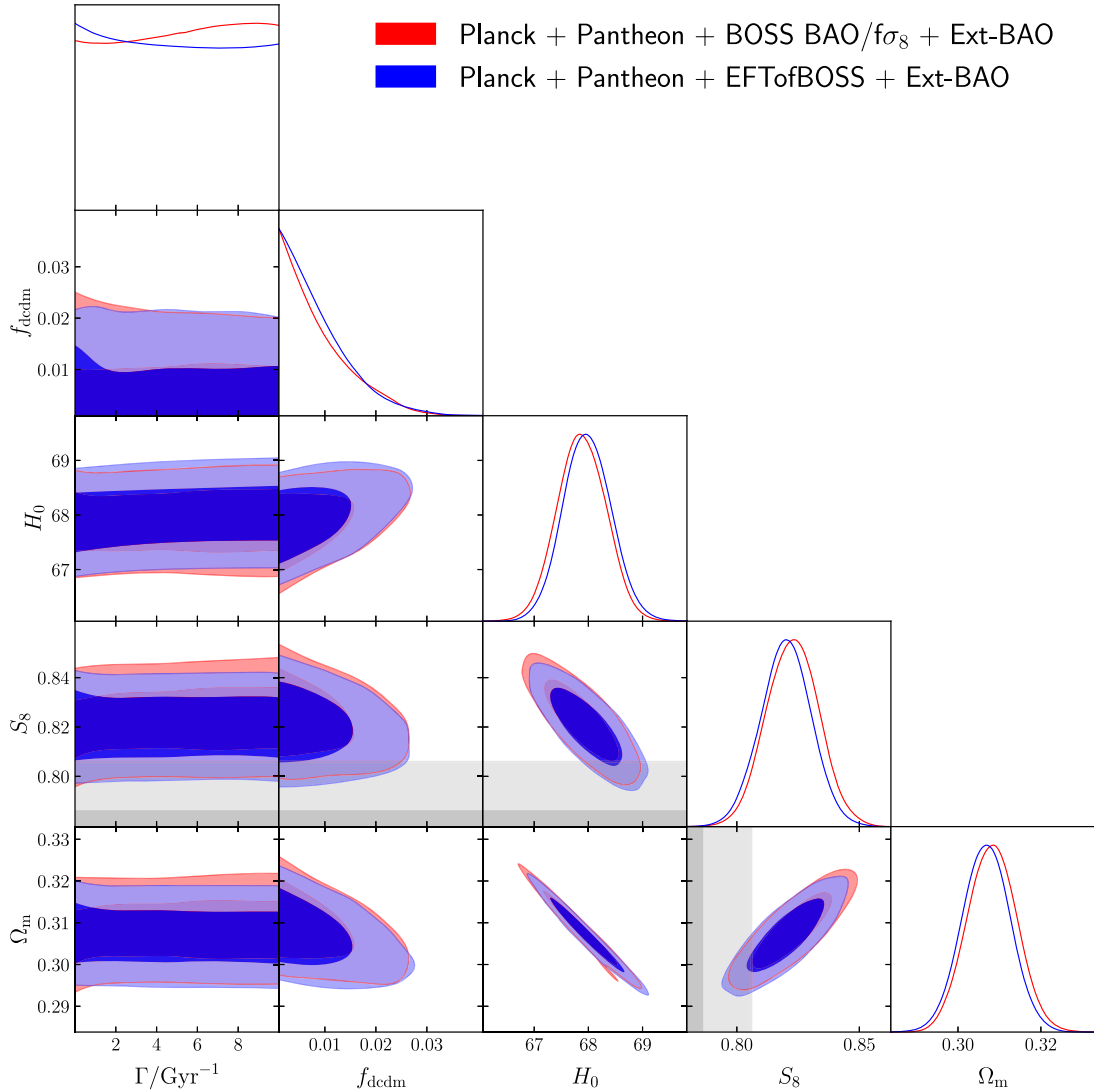
FIG. 7. 2D posterior distributions of the DCDM $\to$ DR model with and without the EFTofBOSS dataset. The gray shaded bands refer to the joint S_8 measurement from KiDS-1000 + BOSS + 2dFLens [158].

which is consistent with the naive analysis presented in Sec. III A 3. Moreover, we show that when adding the S_8 prior, the $\Delta\chi^2$ with respect to ΛCDM is still compatible with zero (and the model does not provide a good fit to the S_8 prior) while the constraints on Γ and f_{dcdm} are largely unaffected. We conclude (as in past studies) that this model does not resolve the S_8 tension.

To summarize our results, and present the most up-to-date constraints on DCDM with massless decay products, in Table V we compare the 95% C.L. limits obtained for f_{dcdm} and τ when successively adding datasets. To obtain the bounds on f_{dcdm} (in the "short-lived" regime), we marginalize over the parameter Γ in the range described above. On the other hand, to obtain the τ limits (in the "very long-lived" regime), we fix $f_{\mathrm{dcdm}} = 1$ in our MCMC analyses, i.e., we assume that all DM decays. Note that, for $f_{\mathrm{dcdm}} \to 1$, one can interpret our constraints as a limit on

the ratio τ/f_{dcdm}, as discussed in Ref. [80]. From Table V, one can deduce the following:

(i) The strongest constraints are obtained when considering $Planck$ + Pantheon + BOSS BAO/$f\sigma_8$ + Ext-BAO (no Ly-α). In that case, we find $f_{\mathrm{dcdm}} < 0.0190$ (in the short-lived regime), and $\tau/f_{\mathrm{dcdm}} > 260.4$ Gyr (for $f_{\mathrm{dcdm}} \to 1$).

(ii) On the other hand, the inclusion of Ly-α BAO data slightly reduces the constraints. This is consistent with the fact that these data are compatible with ΛCDM only at the 1.7σ level [165,166], favoring lower energy density at high-z [168]. Additionally, we find that constraints with the EFTofBOSS data are the same as those with the standard redshift space distortion $f\sigma_8$ information. Our fiducial constraints, including all data, are therefore $f_{\mathrm{dcdm}} < 0.0216$, and $\tau/f > 249.6$ Gyr.

TABLE IV. The mean (best-fit) $\pm 1\sigma$ errors of the cosmological parameters from our $Planck + \text{Pantheon} + \text{EFTofBOSS} + \text{Ext-BAO}$ and $Planck + \text{Pantheon} + \text{EFTofBOSS} + \text{Ext-BAO} + S_8$ analyses for the DCDM $\to$ DR model. For each dataset we also report its best-fit χ^2, and the $\Delta\chi^2$ with respect to the analogous ΛCDM best-fit model.

	DCDM $\to$ DR	
Parameter	w/EFTofBOSS	w/EFTofBOSS $+ S_8$
$\Gamma/[\text{Gyr}^{-1}]$	Unconstrained (4.8)	Unconstrained (5.8)
f_{dcdm}	$<0.0216(1.62 \times 10^{-4})$	$<0.0242(1.67 \times 10^{-4})$
$100\omega_b$	$2.236(2.244) \pm 0.015$	$2.241(2.248)^{+0.016}_{-0.015}$
ω_{cdm}	$0.1187(0.1191) \pm 0.0010$	$0.1180(0.1184)^{+0.001}_{-0.00093}$
$H_0/\,[\text{km/s/Mpc}]$	$67.98(67.77)^{+0.46}_{-0.48}$	$68.30(68.10)^{+0.44}_{-0.47}$
$\ln(10^{10}A_s)$	$3.051(3.049)^{+0.015}_{-0.016}$	$3.047(3.045)^{+0.015}_{-0.016}$
n_s	$0.9650(0.9671)^{+0.0042}_{-0.004}$	$0.9660(0.9687)^{+0.0044}_{-0.0043}$
τ_{reio}	$0.0577(0.0572)^{+0.0073}_{-0.0079}$	$0.0562(0.0557)^{+0.0074}_{-0.0077}$
Ω_m	$0.3069(0.3097) \pm 0.0061$	$0.3026(0.3050)^{+0.0059}_{-0.0057}$
σ_8	$0.8110(0.8101)^{+0.0063}_{-0.0066}$	$0.8071(0.8061)^{+0.0062}_{-0.0063}$
S_8	$0.82(0.82) \pm 0.01$	$0.811(0.813)^{+0.0097}_{-0.0095}$
$\chi^2_{\min}$	3927.0	3933.0
$\chi^2_{\min}(\text{DCDM}) - \chi^2_{\min}(\Lambda\text{CDM})$	0.0	0.0
$Q_{\text{DMAP}} \equiv \sqrt{\chi^2_{\min}(\text{w}/S_8) - \chi^2_{\min}(\text{w/o }S_8)}$	2.4σ	

TABLE V. The 95% C.L. limit on f_{dcdm} for the standard DCDM $\to$ DR analysis, and the 95% C.L. limit on τ for the DCDM $\to$ DR analysis where f_{dcdm} is fixed to the unit. Let us recall that "Ext-BAO" refers to the BAO measurements from 6dFGS, SDSS DR7, and the joint constraints from eBOSS DR14 Ly-α autocorrelation and cross-correlation. For some datasets we removed the Ly-α constraints ("no Ly-α") to explicitly show its impact.

	DCDM $\to$ DR	
Datasets	f_{dcdm}	τ (for $f_{\text{dcdm}} = 1$)
Planck	<0.0205	>246.3 Gyr
Planck + Pantheon + Ext-BAO (no Ly-α)	<0.0203	>248.4 Gyr
Planck + Pantheon + BOSS BAO/$f\sigma_8$ + Ext-BAO (no Ly-α)	<0.0190	>260.4 Gyr
Planck + Pantheon + BOSS BAO/$f\sigma_8$ + Ext-BAO	<0.0219	>250.0 Gyr
Planck + Pantheon + EFTofBOSS + Ext-BAO	<0.0216	>249.6 Gyr

(iii) Our constraints are somewhat different than those derived in Ref. [83], which considering *Planck* 2018 + BAO data (see Table 2 of this reference) found $f_{\text{dcdm}} < 0.0262$ at 95% C.L. and $\tau/f_{\text{dcdm}} > 268.8$ Gyr. Our constraints are stronger on f_{dcdm}, compatible with the fact that we include more data, but weaker on τ, which may be explained by the fact that their posteriors never quite reach $f_{\text{dcdm}} \sim 1$, as necessary to derive constraints in the very long-lived regime.

C. Warm dark matter decay products

We now turn to the case of the DCDM $\to$ WDM + DR model, described by the parameters $\Gamma = \tau^{-1}$, the decay rate of DCDM, and ε, the fraction of DCDM rest mass energy converted into DR. Note that in this section, we trade the density of DM today, ω_{cdm}, for the initial density of DM (before decays occur) at $a \to 0$, $\omega_{\text{dcdm}}^{\text{ini}}$. For a stable particle, we simply have $\omega_{\text{dcdm}}^{\text{ini}} \equiv \omega_{\text{cdm}}$ as defined previously. In the MCMC analyses, we imposed logarithmic priors[14] on ε and Γ, and a flat prior on $\omega_{\text{dcdm}}^{\text{ini}}$:

$$-4 \leq \log_{10}(\Gamma/[\text{Gyr}^{-1}]) \leq 1,$$
$$-4 \leq \log_{10}(\varepsilon) \leq \log_{10}(0.5),$$
$$0 \leq \omega_{\text{dcdm}}^{\text{ini}} \leq 1.$$

We present our results for the analyses with and without S_8 prior in Table VI, while the χ^2 of the EFTofBOSS data of these analysis are reported in Table VII. All relevant χ^2 per experiment are given in Appendix D. In Fig. 8,

[14]For discussions about the impact of prior choices, see the appendix of Ref. [77].

TABLE VI.   The mean (best-fit) $\pm 1\sigma$ errors of the cosmological parameters from our *Planck* + Pantheon + EFTofBOSS + Ext-BAO and *Planck* + Pantheon + EFTofBOSS + Ext-BAO + S_8 analyses for the DCDM $\rightarrow$ WDM + DR model. For each dataset we also report its best-fit χ^2, and the $\Delta\chi^2$ with respect to the analogous ΛCDM best-fit model.

	DCDM $\rightarrow$ WDM + DR	
Parameter	w/EFTofBOSS	w/EFTofBOSS + S_8
$\log_{10}(\Gamma/[\mathrm{Gyr}^{-1}])$	Unconstrained (−2.98)	$2.21(-2.08)^{+1.5}_{-0.6}$
$\log_{10}(\varepsilon)$	Unconstrained (−3.84)	$-2.30(-1.92)^{+0.84}_{-1.10}$
$100\omega_b$	$2.242(2.245)^{+0.014}_{-0.014}$	$2.245(2.242)^{+0.014}_{-0.015}$
ω_{dcdm}^{ini}	$0.1192(0.1190)^{+0.00089}_{-0.0009}$	$0.1188(0.1192)^{+0.00084}_{-0.00099}$
$H_0/$ [km/s/Mpc]	$67.78(67.82)^{+0.41}_{-0.42}$	$67.97(67.73)^{+0.44}_{-0.42}$
$\ln(10^{10}A_s)$	$3.049(3.051)^{+0.015}_{-0.016}$	$3.046(3.052)^{+0.015}_{-0.016}$
n_s	$0.9668(0.9679) \pm 0.0039$	$0.9676(0.9670) \pm 0.0039$
τ_{reio}	$0.0571(0.0584)^{+0.0071}_{-0.0080}$	$0.0564(0.0584)^{+0.0074}_{-0.0077}$
Ω_m	$0.3090(0.3089)^{+0.0055}_{-0.0057}$	$0.3064(0.3094)^{+0.0055}_{-0.0058}$
σ_8	$0.806(0.811)^{+0.012}_{-0.014}$	$0.790(0.763)^{+0.027}_{-0.010}$
S_8	$0.818(0.823)^{+0.016}_{-0.012}$	$0.798(0.775)^{+0.025}_{-0.012}$
χ^2_{min}	3927.0	3929.3
$\chi^2_{min}(\mathrm{DCDM}) - \chi^2_{min}(\Lambda\mathrm{CDM})$	0.0	−3.8
$Q_{DMAP} \equiv \sqrt{\chi^2_{min}(\mathrm{w}/S_8) - \chi^2_{min}(\mathrm{w}/\mathrm{o}S_8)}$	1.5σ	

TABLE VII. χ^2 of each sky-cut of the EFTofBOSS dataset for our *Planck* + Pantheon + EFTofBOSS + Ext-BAO and *Planck* + Pantheon + EFTofBOSS + Ext-BAO + S_8 analyses for ΛCDM, DCDM $\rightarrow$ DR and DCDM $\rightarrow$ WDM + DR models.

	ΛCDM		DCDM $\rightarrow$ DR		DCDM $\rightarrow$ WDM + DR	
	w/EFTofBOSS	w/EFTofBOSS + S_8	w/EFTofBOSS	w/EFTofBOSS + S_8	w/EFTofBOSS	w/EFTofBOSS + S_8
$\chi^2_{\mathrm{CMASS\ NGC}}$	40.3	39.2	40.4	39.2	40.2	40.8
$\chi^2_{\mathrm{CMASS\ SGC}}$	44.0	44.3	44.0	44.3	44.1	43.8
$\chi^2_{\mathrm{LOWZ\ NGC}}$	33.5	33.5	33.5	33.5	33.5	33.7
$\chi^2_{\mathrm{EFTofBOSS}}$	117.8	117.0	117.9	117.0	117.8	118.3
p-value	0.54	0.56	0.49	0.51	0.49	0.47

we display the 1D and 2D posteriors of $\{\log_{10}(\Gamma/[\mathrm{Gyr}^{-1}]),$ $\log_{10}(\varepsilon), H_0, S_8, \Omega_m\}$ for the DCDM $\rightarrow$ WDM + DR model with and without the EFTofBOSS dataset, always including the S_8 prior. Posteriors without the S_8 prior are shown in Appendix C.

1. Estimating the tension with the S_8 measurement

Without the S_8 prior, the total χ^2 does not show any improvement (see Table VI) and the data do not favor the DCDM $\rightarrow$ WDM + DR model. In fact, in the absence of the S_8 prior, it seems that one could derive apparently strong constraints on these models.[15] Yet,

once the S_8 likelihood is included, we find $\Delta\chi^2 = -3.8$ (for 2 extra degrees of freedom) at virtually no cost in χ^2 for other likelihoods (see Appendix D): the inclusion of the S_8 prior helps in opening up the degeneracy with the DCDM parameters, without degrading the fit to the host of cosmological data, as stressed in Refs. [70,77].

Nevertheless, the DCDM model is not statistically favored over ΛCDM, as the preference over ΛCDM is currently solely driven by the low S_8 prior, for which we have used a value only in mild $\sim 2.4\sigma$ tension with the ΛCDM prediction.[16] We can estimate the residual tension between datasets within the various models by computing the "difference in maximum a posteriori"

---

[15]In Ref. [77], it was shown through a mock data analysis that *Planck* data alone could not detect the best-fit model required to explain the S_8 tension, artificially leading to strong constraints on the DCDM model.

[16]Different S_8 priors would lead to different preferences. The preference could also be made stronger at fixed ε (see Ref. [77]).
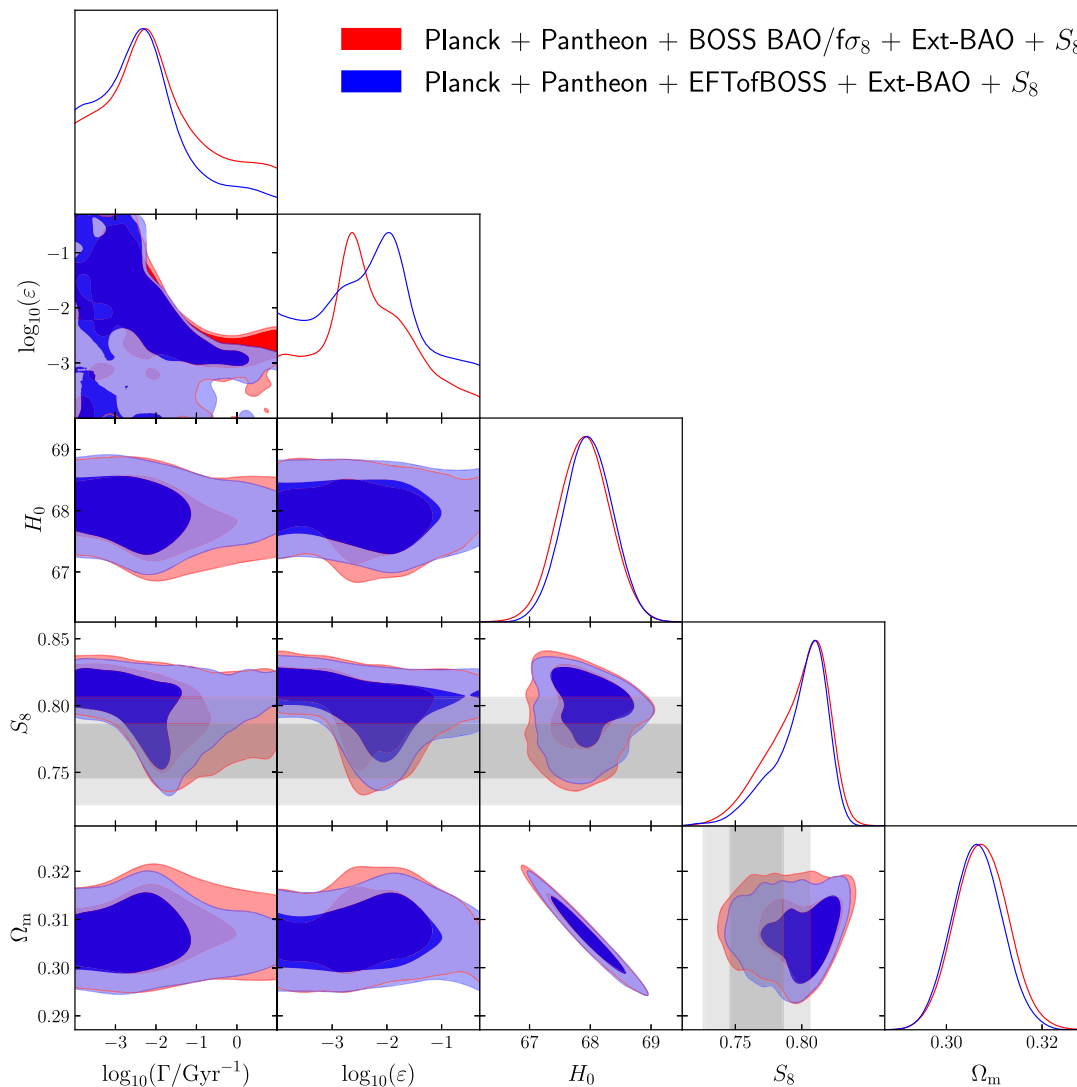
FIG. 8. 2D posterior distributions of the DCDM → WDM + DR model with and without the EFTofBOSS dataset. We took into account the S_8 prior from KIDS-1000 for these two MCMC analyses. The gray shaded bands refer to the joint S_8 measurement from KiDS-1000 + BOSS + 2dFLens.

(Q_{DMAP} statistics [169]) between the χ^2 obtained with and without the S_8 prior. The tension estimator[17] at their MAP point gives $Q_{\text{DMAP}} = 1.5\sigma$ in the DCDM → WDM + DR model, as compared to 2.4σ in the ΛCDM and DCDM → DR models.

---

[17]In general, Q_{DMAP} is computed as the difference of effective $\chi^2 = -2\text{Log}\mathcal{L}(\theta^{\text{MAP}})$, where $\mathcal{L}(\theta^{\text{MAP}})$ is the likelihood evaluated on the maximum *a posteriori* θ^{MAP}, between the χ^2 obtained in the combined analysis and the sum of the χ^2 obtained in the individual analyses. For Gaussian $\mathcal{L}$, it is distributed as a χ^2 distribution with $N_1 + N_2 - N_{12}$ degrees of freedom (d.o.f.), where N_i refers to the number of d.o.f. in the individual ($i = 1, 2$) and combined analysis ($i = 12$). In the case of the combination of *Planck* and a Gaussian prior on S_8, it follows a χ^2 distribution with one d.o.f., and the tension can be evaluated as $Q_{\text{DMAP}} \equiv \sqrt{\chi^2_{\text{min}}(\text{w}/S_8) - \chi^2_{\text{min}}(\text{w/o }S_8)}$.

2. Impact of EFTofBOSS data

Comparing to results without the EFTofBOSS data, for which we get[18] $\Delta\chi^2 = -4.4$, we find that the $\Delta\chi^2$ is only mildly degraded by the inclusion of EFTofBOSS data. More precisely, the χ^2 of the total EFTofBOSS data for the DCDM → WDM + DR model, given in Table VII, is only slightly larger than that for ΛCDM ($\Delta\chi^2 = 1.3$) despite a much lower $S_8 \simeq 0.775$ (at the best fit) which yields a very good fit of the KiDS-1000 prior. Comparing to the analysis with the BAO/$f\sigma_8$ measurement from BOSS-DR12 (also presented in Appendix D), we note that these "compressed" data already showed a minor degradation of χ^2 compared to

---

[18]This number is different from that quoted in Refs. [70,77] because we recall that we make use of a different S_8 prior from KiDS-1000 alone, which does not include information from BOSS data and therefore has larger error bars.

ΛCDM ($\Delta\chi^2 = 1.1$). We conclude that BOSS-DR12 data are in good agreement with the DCDM $\rightarrow$ WDM + DR model, but have a non-negligible impact, as the naive analysis presented in Sec. III B 3 suggested.

More precisely, one can see in Fig. 8 that the main impact of EFTofBOSS data is to cut in the $\log_{10}(\Gamma/\text{Gyr}^{-1}) - \log_{10}(\varepsilon)$ degeneracy, excluding too large values of $\log_{10}(\Gamma/\text{Gyr}^{-1})$. In Appendix E we show that including the EFTofBOSS data does not shift the ΛCDM parameters. Therefore, the EFTofLSS significantly improves the constraints on the $\tau = \Gamma^{-1}$ parameter at 1σ:

$$1.61 < \log_{10}(\tau/\text{Gyr}) < 3.71 \quad (\text{w/EFTofBOSS}),$$

to be compared with

$$1.31 < \log_{10}(\tau/\text{Gyr}) < 3.82 \quad (\text{w/o EFTofBOSS}).$$

Additionally, we observe a notable evolution of the DCDM parameters of the best-fit model compared to the analysis without EFTofBOSS (and with the BAO/$f\sigma_8$ measurement from BOSS-DR12 instead): the best-fit model, with the inclusion of the S_8 likelihood, now has $\Gamma = 0.0083$ Gyr^{-1} ($\tau = 120$ Gyr) and $\varepsilon = 0.012$, while previously $\Gamma = 0.023$ Gyr^{-1} ($\tau = 43$ Gyr) and $\varepsilon = 0.006$. This means that EFTofBOSS data favors longer lived DM

models and therefore a smaller fraction of WDM today $f_{\text{wdm}} \equiv \bar{\rho}_{\text{wdm}}/(\bar{\rho}_{\text{dcdm}} + \bar{\rho}_{\text{wdm}}) \simeq 10\%$ compared to $f_{\text{wdm}} \simeq 27\%$ previously, but a significantly larger kick velocity $v_{\text{kick}}/c \simeq \varepsilon$ (and therefore a larger free-streaming scale).

It is instructive to compare these numbers with recent constraints derived from observations of Milky Way satellites by the DES collaboration [170]. These constraints exclude $\log_{10}(\Gamma/\text{Gyr}^{-1}) \gtrsim -1.5$ for $\log_{10}(v_{\text{kick}}/c) \simeq \log_{10}(\varepsilon) \gtrsim -4$. The best-fit model of our EFTofBOSS analysis, and a large fraction of the 68% C.L., lie well within the allowed region, but these observations certainly provide a crucial test of the DCDM cosmology, as a deficit of satellites compared to ΛCDM is expected in this model.

3. Towards high-accuracy measurements of the galaxy power spectrum

To gauge the importance of future surveys in constraining the DCDM $\rightarrow$ WDM + DR model, we show in Fig. 9 the residuals of the monopoles and quadrupoles of the galaxy power spectrum between the DCDM $\rightarrow$ WDM + DR and ΛCDM models. One can see that there are subpercent differences between the models that gives us hope to probe the DCDM model further. Indeed, future galaxy clustering power spectrum data with higher precision and measurements at additional redshift bins such as
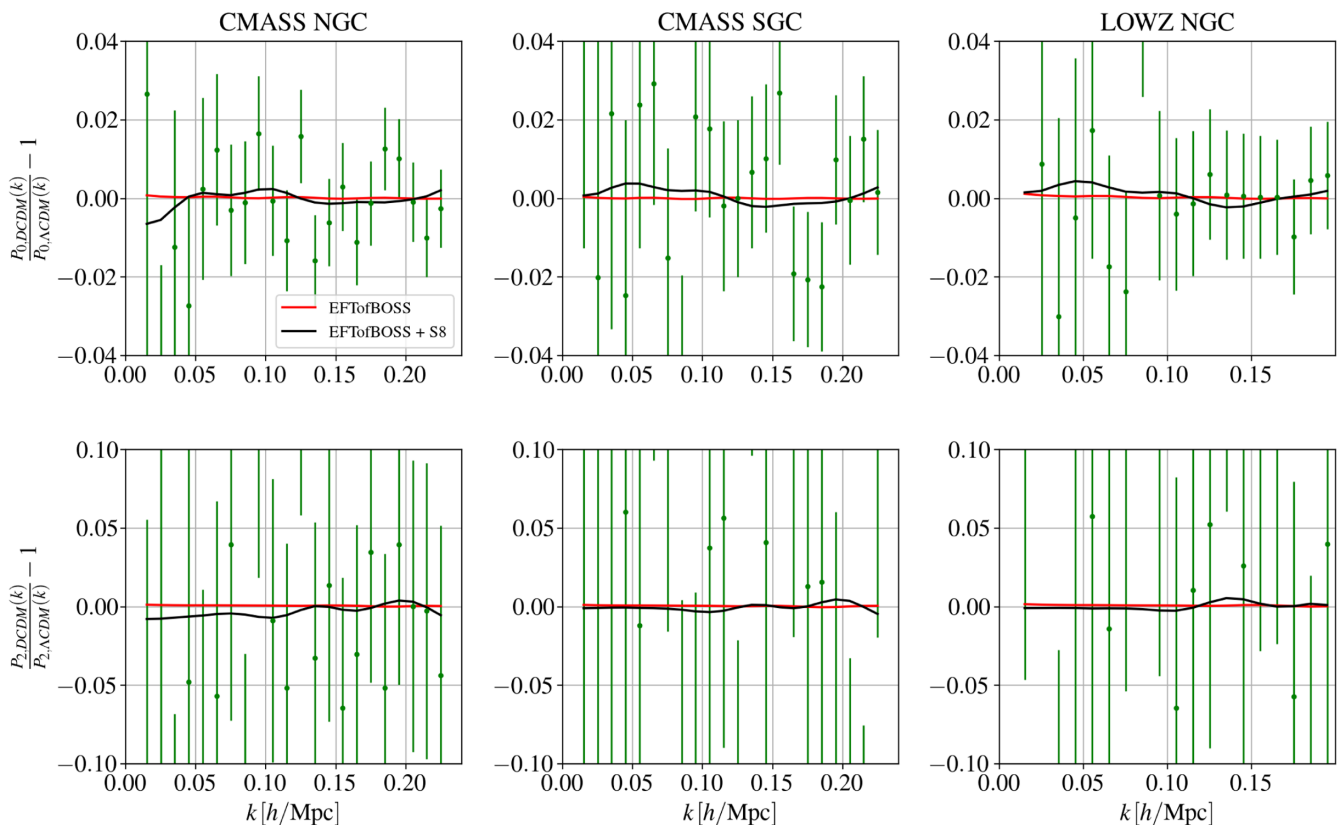

FIG. 9. Residuals of the monopole and the quadrupole of the DCDM $\rightarrow$ WDM + DR model for EFTofBOSS data and EFTofBOSS data + S_8 prior. We normalized these residuals as well as the data with the ΛCDM best fit (EFTofBOSS data).
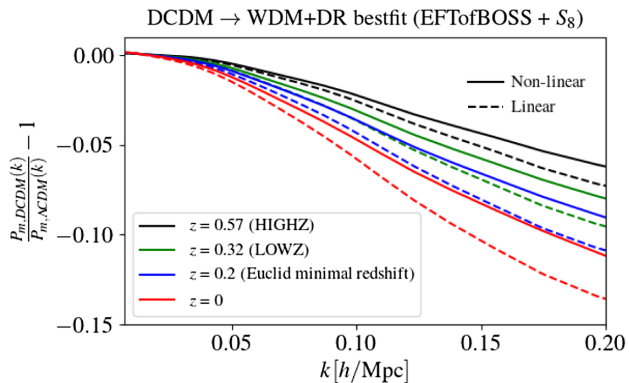
FIG. 10. Residuals of linear (dashed lines) and nonlinear (solid line) matter power spectrum of the DCDM → WDM + DR model (EFTofBOSS data + S_8 prior) for $z = 0$, 0.2 (Euclid minimal redshift), 0.32 (effective redshift of the LOWZ sky-cut) and 0.57 (effective redshift of the HIGHZ sky-cut). We normalized these residuals with the ΛCDM best fit (EFTofBOSS data).

Euclid [137], VRO [138] and DESI [171] have an expected sensitivity that should allow us to detect these mild differences. In order to estimate the impact of future observations on the preference of the DCDM → WDM + DR model with respect to the ΛCDM model, we plot in Fig. 10 the residuals of the nonlinear matter power spectrum[19] between the best fit of the DCDM → WDM + DR model (for the EFTofBOSS + S_8 analysis) and ΛCDM model (for the EFTofBOSS analysis). We represent it for different redshifts, starting at the minimal redshift probed by an experiment like Euclid [137]. Note that at the level of the nonlinear matter power spectrum, the suppression with respect to the ΛCDM model at $z = 0.32$ and $z = 0.57$ corresponding to current observations is more than 1 order of magnitude stronger than what is seen in the residual of the monopole and quadrupole of the galaxy power spectrum (see Fig. 9). This is due to the impact of the degeneracy between the DCDM parameters and the EFT galaxy bias parameters, which can counteract the effect of the DCDM decay in the galaxy power spectrum. This shows that current theoretical uncertainties associated with galaxy bias parameters limit the ability to use galaxy (clustering) surveys to probe the DCDM model, and represent a potential challenge to fully exploit future surveys. Additionally, we observe that as z decreases, the deviation from ΛCDM increases significantly because of the production of WDM through the decay. We keep for future work to check through dedicated forecasts whether accumulation of low redshift data, as well as the reduction of error bars, will allow us to firmly detect or exclude the DCDM → WDM + DR model that resolves the S_8 tension.

---

[19]We set here $c_s = 1$, which is an effective parameter of the one-loop correction that can be interpreted as the effective sound speed of the dark matter.

V. CONCLUSIONS

In this paper, we have confronted two models of DCDM with BOSS DR12 galaxy power spectrum data [139] as described by the EFTofLSS from Refs. [122–128]. We focused first on a model where a fraction of dark matter decays into dark radiation, the DCDM → DR model, and second on a model where all the dark matter decays into warm massive particles and dark radiation particles, the DCDM → WDM + DR model. The latter model was recently suggested as a possible resolution to the S_8 tension, the mismatch between the determination of the S_8 parameter from the *Planck* CMB power spectrum [3] and from weak lensing surveys by KiDS [7,158], CFHTLenS [172] and DES [8]. We presented in Sec. III the first calculation of the nonlinear (matter and galaxy) power spectra in DCDM models making use of recent progresses in the EFTofLSS. We then confronted in Sec. IV these two models to a compilation of *Planck* TTTEEE and lensing power spectra, BAO data from BOSS and eBOSS (including Ly-α data), uncalibrated luminosity distance to SN1a from the Pantheon catalog [162], as well as measurements of the monopole and quadrupole of the galaxy power spectrum for three different sky-cuts of BOSS-DR12 (see Ref. [142]), namely LOWZ NGC, CMASS NGC and CMASS SGC [139]. We compared the use of either the BAO/$f\sigma_8$ from that same release, or the full shape of the galaxy power spectrum. Additionally, we tested the ability of these models to resolve the S_8 tension by performing analyses with and without prior on S_8 as measured by KiDS [7]. Our results can be summarized as follows:

(i) We have derived the most up-to-date bound on the fraction of decaying dark matter f_{dcdm}, which is now $f_{dcdm} < 0.0216$ for short-lived DCDM. We have also updated constraints on the lifetime of dark matter for the case where $f_{dcdm} \rightarrow 1$, namely $\tau/f_{dcdm} >$ 249.6 Gyr. However, we have found that the EFTofLSS does not provide significantly better constraints to the cosmological parameters for the DCDM → DR model, compared to the use of the standard BAO/$f\sigma_8$ data. In agreement with past studies, we have found that these models do not help neither for the S_8 nor for the H_0 tension, and the inclusion of EFTofBOSS data does not alter that conclusion.

(ii) The DCDM → WDM + DR model can explain the low S_8 value measured by KiDS-1000 while preserving the goodness of fit to other dataset, including EFTofBOSS data. The residual tension is 1.5σ compared to 2.4σ in the ΛCDM model. Nevertheless, the model is not statistically favored over ΛCDM ($\Delta\chi^2 = -3.8$ for 2 degrees of freedom, roughly corresponding to 1.5σ). The inclusion of EFTofBOSS data only marginally affects the preference.

(iii) EFTofBOSS data however do significantly improve the 1-σ constraint on the DCDM lifetime for the

DCDM → WDM + DR model, and when combined with the S_8 prior, we now obtain $\log_{10}(\tau/\mathrm{Gyr}) = 2.21^{+1.5}_{-0.6}$ compared to $\log_{10}(\tau/\mathrm{Gyr}) = 1.92^{+1.9}_{-0.61}$ without the EFTofBOSS. The constraints on $\log_{10}(\varepsilon)$ are however slightly weaker than with BAO/$f\sigma_8$ measurements.

(iv) The EFTofBOSS data also affects the best-fit model which, with the inclusion of the S_8 likelihood, corresponds to a longer lived DM with $\tau = 120$ Gyr (compared to $\tau = 43$ Gyr previously) and a larger kick velocity $v_{\mathrm{kick}}/c \simeq \varepsilon = 1.2\%$ (compared to $v_{\mathrm{kick}}/c \simeq 0.6\%$ previously).

Looking forward, we expect future galaxy clustering power spectrum data, with higher precision and measurements at additional redshift bins such as Euclid [137], VRO [138] and DESI [171], to provide us with exquisite sensitivity to DM decays into an invisible sector whether massive or massless. Moreover, as the error bars decrease, it will likely be necessary to identify and account for the corrections to be made to the EFTofLSS in order to capture all the specific effects of the DCDM → WDM + DR model. Following Ref. [156] for the case of massive neutrinos, it will be important to determine the one-loop terms and associated counterterms of the mildly nonlinear galaxy power spectrum caused by the WDM contribution to the linear matter power spectrum (which we have argued in Appendix B to likely be small compared to current error bars). We keep for future work to test whether these surveys will be able to firmly detect or exclude the DCDM → WDM + DR model that resolves the S_8 tension.

ACKNOWLEDGMENTS

APPENDIX A: COMPARISON BETWEEN THE EFTofLSS AND N-BODY METHODS FOR THE DCDM → DR MODEL

In this Appendix, we compare the nonlinear matter power spectrum obtained through the EFTofLSS method with the results of dedicated N-body simulations performed in Ref. [151]. The authors of Ref. [151] have determined a fitting formula which describes the correction to the nonlinear matter power spectrum due to the DM decay compared to the ΛCDM model, as a function of τ, f_{dcdm}, and the redshift z. In Fig. 11, we compare this fitting formula, where we set $\tau = 32$ Gyr and $z = 0$ and vary $f_{\mathrm{dcdm}} \in [0, 1]$, with the linear matter power spectrum of the CLASS code (left panel), and with the nonlinear matter power spectra from both the CLASS-PT and PyBird codes (right panel). Here, we set the ΛCDM parameters to the values used in Ref. [151]. The left panel of this figure is intended as a reproduction of Fig. 1 of this reference for direct comparison, while the right panel presents the comparison of interest. Indeed, from the right panel of Fig. 11, one can clearly see that (i) the CLASS-PT and PyBird codes give very similar power spectra for the
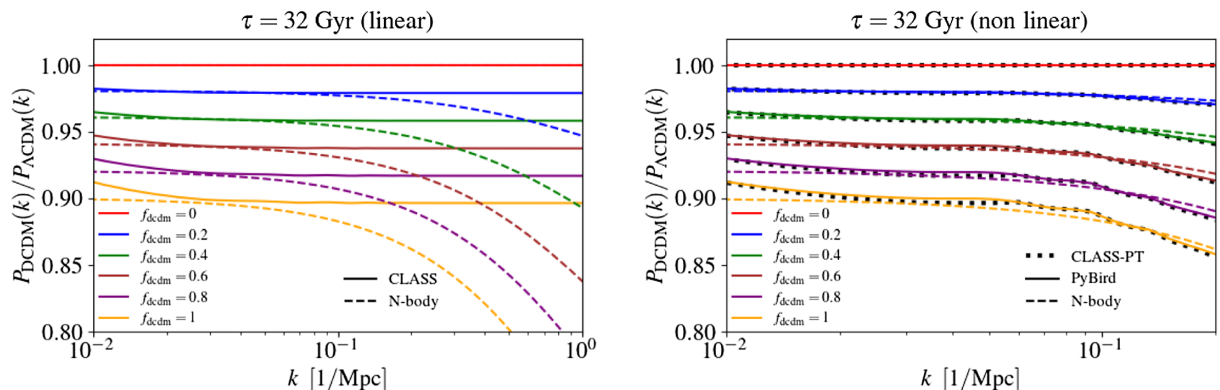

FIG. 11.   Comparison between the residuals of the nonlinear matter power spectra predicted by the N-body simulation and the residuals of the linear matter power spectra predicted by the CLASS code on the one hand (left panel), and the residuals of the nonlinear matter power spectra predicted by the CLASS-PT and PyBird codes on the other hand (right panel). We compute these power spectra for $z = 0$ and for $\tau = 32$ Gyr, while we varied f_{dcdm} from 0 to 1 with a step of 0.2.
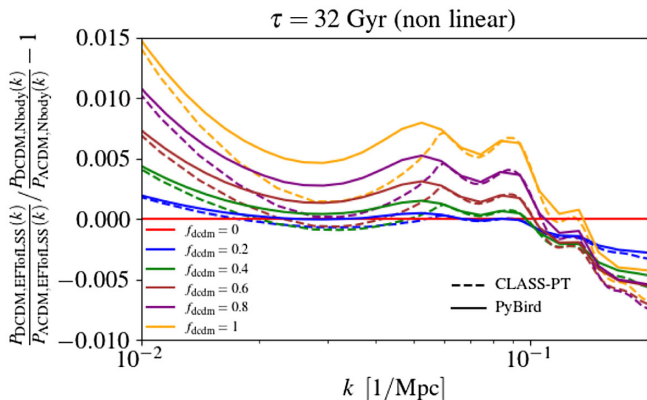
FIG. 12. Ratio between residuals of the nonlinear matter power spectra obtained from the N-body simulation and those obtained from the CLASS-PT and the PyBird codes for $z = 0$, $\tau = 32$ Gyr and f_{dcdm} varying from 0 to 1 with a step of 0.2.

DCDM → DR model,[20] and (ii) the deviation from ΛCDM predicted in these two EFTofLSS codes is very close to that obtained through N-body simulation. In order to determine more precisely the deviations between the EFTofLSS and the N-body methods, we plot, in Fig. 12, the ratio between the residuals obtained with the N-Body simulation and those obtained with the CLASS-PT and PyBird codes. One can see that the difference is below the ∼1% level until $k \sim 0.2h \ \mathrm{Mpc}^{-1}$ (the maximum k at which the EFTofLSS is valid at one-loop order for a small z). Let us note that the difference between the N-body simulation and the EFTofLSS power spectrum for $k \lesssim 0.02h \ \mathrm{Mpc}^{-1}$ is not relevant; it is merely due to the fact that the N-body fitting formula does not encode this behavior for low k (see [151]), but this k range is well within the linear regime and does not necessitate a correction. Let us also remark that the lower f_{dcdm} (or the longer τ), the smaller the difference between the residuals from the N-body and those from the EFTofLSS method. Since current constraints only allow small values of $f_{\mathrm{dcdm}} \lesssim 2.5\%$ or large lifetime $\tau \gtrsim 240$ Gyr, it is safe to use the PyBird (or CLASS-PT) code in their current form to describe the DCDM → DR model. This good agreement between the EFT approach and the N-body simulation, despite having made no change to the EFT modeling, may appear surprising at first sight. However, there is a fairly intuitive argument as to why the DM equations (and therefore the EFT formalism) should receive only minor corrections from the presence of a nonzero decay term. This is because, in the synchronous gauge at linear order, the DCDM equations are strictly identical to that of CDM: the effect of the decay is happening exactly at the same rate everywhere in space, and therefore cancels out the perturbed continuity and Euler

equations which drive the DCDM perturbed dynamics. Although strictly speaking, the contribution of the decay term may appear at higher order, as we treat the mildly nonlinear regime, it will be subdominant. This explains why we find such a good agreement between N-body simulations and the EFT computation despite not modifying the master equations, the expansion nor the counterterms. Note that this argument is valid irrespective of the mass of the daughter particles as far as the mother particle is concerned. Similarly, corrections to the massless daughter equations may appear, but will likely have only a small impact on the observables given that the massless daughter quickly redshift away compared to other species for decays happening at late times (at times relevant for galaxy surveys).

APPENDIX B: ASSESSING THE VALIDITY OF THE EFTofLSS IN THE DCDM → WDM + DR MODEL

In this Appendix, we discuss the validity of the EFTofLSS in the DCDM → WDM + DR model. In Ref. [156], the EFTofLSS was extended to describe massive neutrinos, an extension to ΛCDM with properties similar to that of the DCDM → WDM + DR model. Indeed, the main issue with employing the EFTofLSS to describe the DCDM → WDM + DR model does not lie in the effect of the decay itself (the effect of the decay on the perturbed equations of the DCDM is identical to that of the DCDM → DR model, which is captured by our formalism as discussed in Appendix A), but rather in the production of a warm massive species which may contribute in a nontrivial way to the power spectrum of galaxies. At the linear level, it was found the massive decay products behave similarly to CDM at wave numbers smaller than the free-streaming scale k_{fs} [with k_{fs} approximately given by Eq. (26)], but is strongly suppressed due to pressure terms at larger wave numbers similarly to WDM and hot DM such as neutrinos. In Ref. [156], the contribution of neutrinos to the total one loop power spectrum was computed, and it was found that the dominant effect is a correction to the dark matter power spectrum that scales like $16f_\nu$, where $f_\nu \equiv \bar{\rho}_\nu / (\bar{\rho}_\nu + \bar{\rho}_{\mathrm{cdm}}) \sim 1\%$, at $k > k_{\mathrm{fs}}$ and roughly half of that at $k < k_{\mathrm{fs}}$. The naive $\mathcal{O}(f_\nu)$ contribution is enhanced by twice the logarithm of the redshift of matter-radiation equality, as neutrinos are present from early times. The log-enhanced contribution represents about 70% of the contribution to the total one loop power spectrum. Additionally, at leading order, counterterms can be captured by simply rescaling the effective DM sound speed c_s^2 and do not necessitate adding new parameters to the dark-matter-only calculation. In the case of the DCDM model, the WDM is produced at much later times. We plot in Fig. 13 (right panel) the redshift $z_{1\%}$ at which the WDM contribution $f_{\mathrm{wdm}} \equiv \bar{\rho}_{\mathrm{wdm}} / (\bar{\rho}_{\mathrm{wdm}} + \bar{\rho}_{\mathrm{dcdm}})$ reaches ∼1%. We also represent the limit at 68% C.L. derived in our

---

[20]We set, in the PyBird and CLASS-PT codes, $c_s = 1$, which is an effective parameter of the one-loop correction that can be interpreted as the effective sound speed of the dark matter.
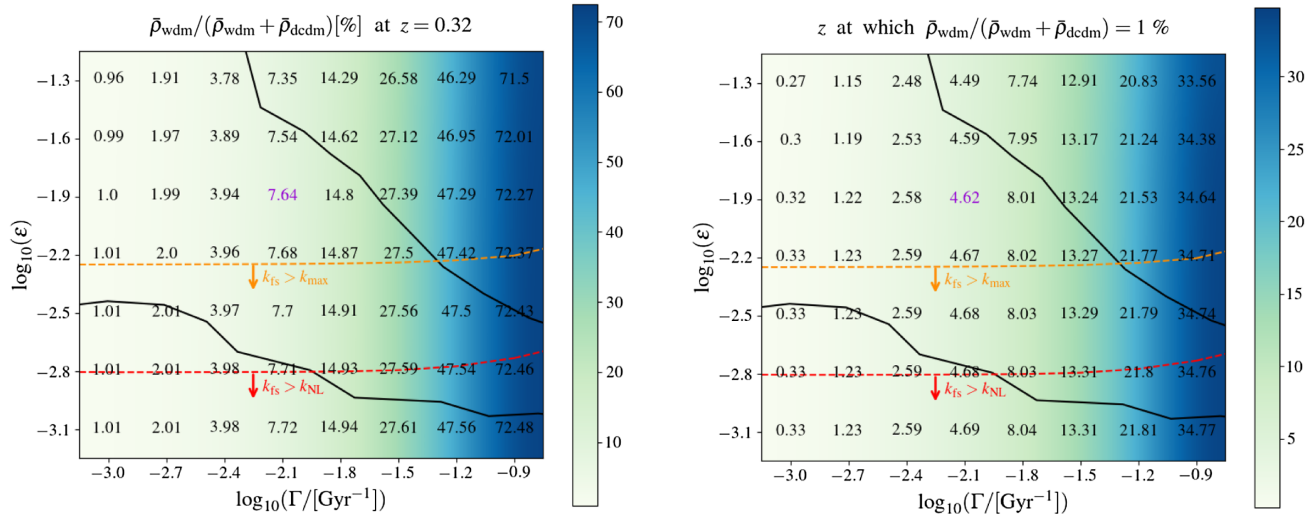
FIG. 13. Values of the WDM fraction at $z = 0.32$ (left panel) and the redshift at which the WDM fraction becomes 1% (right panel), in a region of the $\log_{10}(\varepsilon) - \log_{10}(\Gamma/\text{Gyr}^{-1})$ plane. The ΛCDM parameters are fixed to the best fit from the $Planck$ + Pantheon + EFTofBOSS + Ext-BAO + S_8 analysis. The black lines indicate the 1σ limits of this analysis, while the point highlighted in purple indicates the best fit. All the points below the yellow and red lines correspond to models having a WDM free-streaming wave number k_{fs} larger than $k_{\text{max}} = 0.2h \text{ Mpc}^{-1}$ and $k_{\text{nl}} = 0.7h \text{ Mpc}^{-1}$, respectively.

work. For the best-fit model (shown in purple in the figure), $z_{1\%} \sim 5$. The log enhancement from the ratio of scale factor between $z \sim 5$ and $z_{\text{eff,LOWZ}} = 0.32$ is $\log[(1 + z_{1\%})/(1 + z_0)] \approx 1-2$ compared to the $\log[(1 + z_{\text{eq}})/(1 + z_0)] \approx 8$ in the neutrino study in Ref. [156] that gives the $16f_\nu$ factor. We therefore expect the WDM correction to be comparable to the massive neutrino case even if the energy density (today) ratio is ≈ 10 times larger than neutrinos.

We plot in Fig. 13 (left panel), the fractional contribution of WDM at $z = 0.32$ (the effective redshift of the low-z surveys) as a function of Γ and ε. We also represent the limit at 68% C.L. derived in this work. One can see that it is under $\sim 15\%$ as long as $\log_{10}(\Gamma/[\text{Gyr}^{-1}]) \lesssim -1.8$. Additionally, we show the value of $\varepsilon - \Gamma$ for which the free-streaming scale k_{fs} is equal to the maximum k mode relevant for our analysis of BOSS data ($k_{\text{max}} = 0.2h \text{ Mpc}^{-1}$) and the maximum scale considered in the EFT computation ($k_{\text{nl}} = 0.7h \text{ Mpc}^{-1}$). In a large part of the parameter space favored by our analysis for which f_{wdm} is not small, k_{fs} exceeds k_{max} and therefore corrections should also be minor. An improved EFT treatment including the effect of the massive decay product would be necessary however to describe the power spectrum up to k_{nl}. Given current precision of the data and the large theoretical uncertainty already present, the corrections to our calculation

should be negligible, but more work needs to be done to accurately describe the part of the parameter space with large Γ (and leading to large f_{wdm}), in particular for future surveys which can reach subpercent precision at larger wave numbers.

APPENDIX C: THE ROLE OF THE S_8 PRIOR

In this Appendix, we present 2D posterior distributions obtained with and without the S_8 prior (but with the EFTofBOSS data) in both DCDM cosmologies. In the case of the DCDM $\rightarrow$ DR model, represented in Fig. 14, the impact of the S_8 prior is minor. However, in the case of the DCDM $\rightarrow$ WDM + DR model, represented in Fig. 15, it opens up a degeneracy with $\{\Gamma, \varepsilon\}$ which can lead to low S_8 while preserving the fit to other datasets. Without the S_8 prior, the DCDM model is not favored by $Planck$ data. As discussed in the main text, when the S_8 prior is included, the fit to $Planck$ data is not affected, while the DCDM model can accommodate the lower S_8 value, contrarily to the ΛCDM model. From the Q_{DMAP} statistics [169], we can estimate the residual tension as $Q_{\text{DMAP}} \equiv \sqrt{\chi^2_{\text{min}}(\text{w}/S_8) - \chi^2_{\text{min}}(\text{w}/\text{o } S_8)} = 1.5\sigma$ in the DCDM $\rightarrow$ WDM + DR model, as compared to 2.4σ in the ΛCDM model and DCDM $\rightarrow$ DR model.
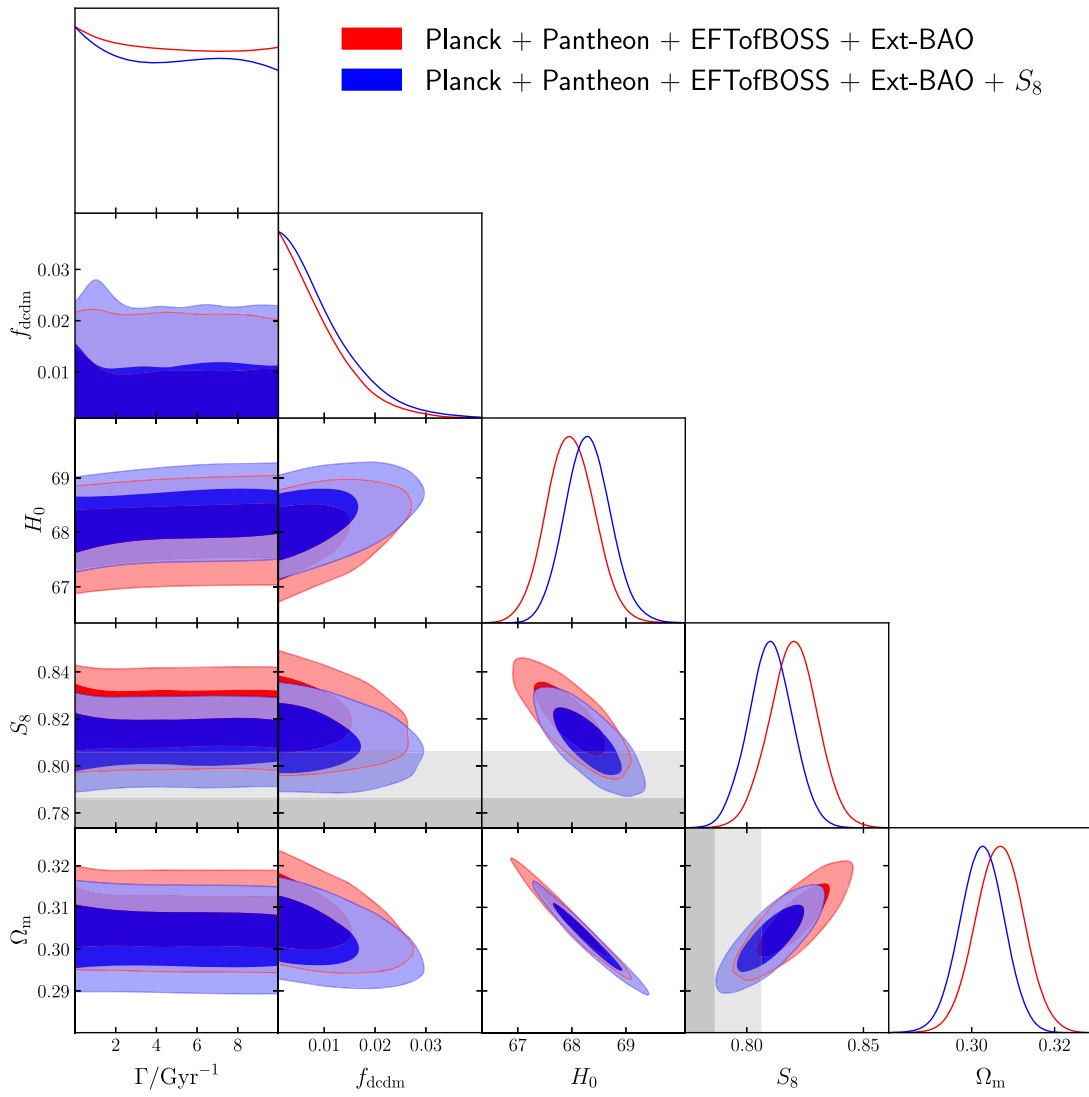
FIG. 14.   2D posterior distributions of the DCDM → DR model reconstructed from an analysis of *Planck*, Pantheon, Ext-BAO and EFTofBOSS data, with (blue) and without (red) the S_8 prior from KiDS-1000. The gray shaded bands refer to the joint S_8 measurement from KiDS-1000 + BOSS + 2dFLens.
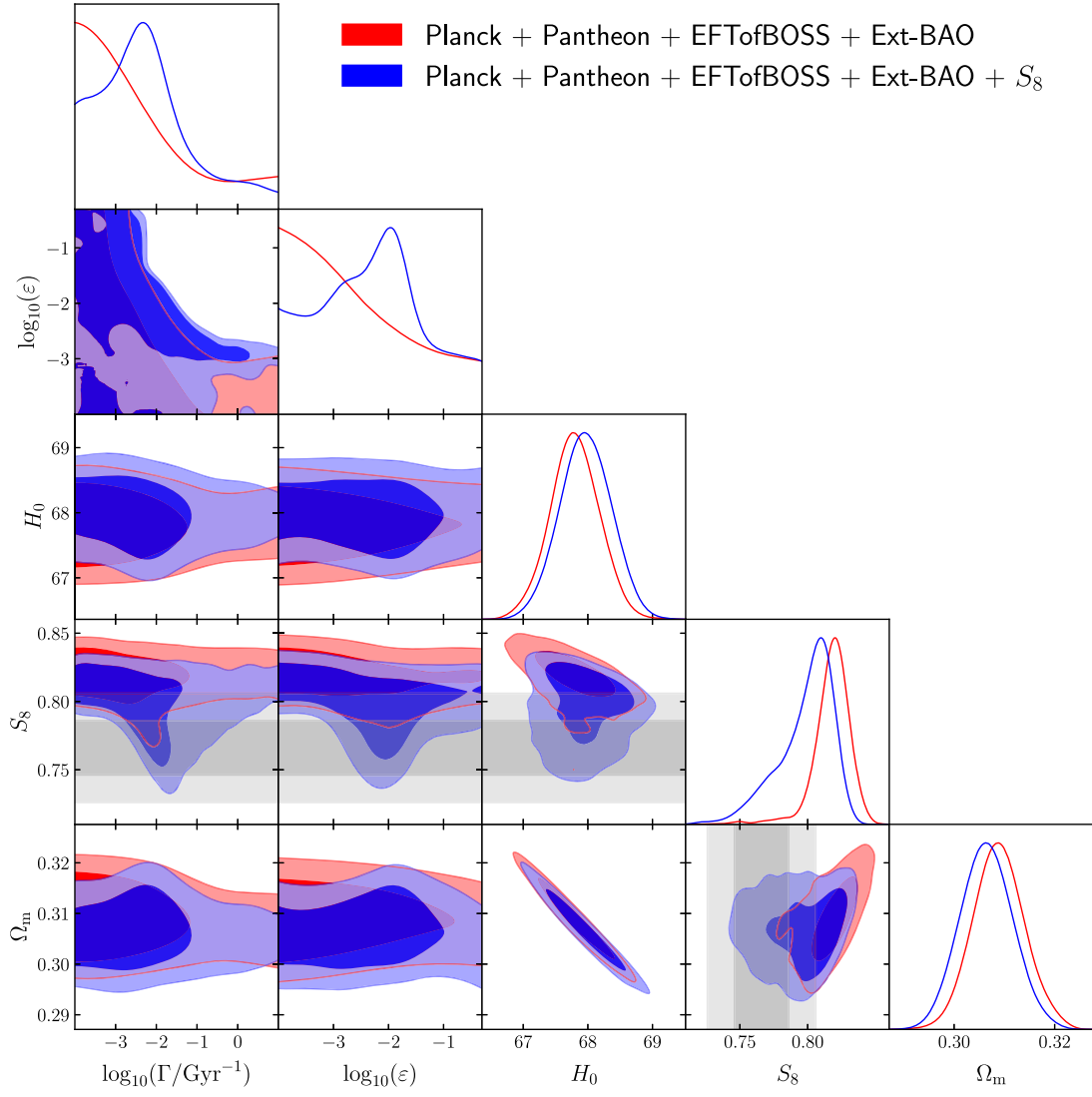
FIG. 15.   2D posterior distributions of the DCDM → WDM + DR model reconstructed from an analysis of *Planck*, Pantheon, Ext-BAO and EFTofBOSS data, with (blue) and without (red) the S_8 prior from KiDS-1000. The gray shaded bands refer to the joint S_8 measurement from KiDS-1000 + BOSS + 2dFLens.

TABLE VIII. χ^2 of each dataset for our $Planck$ + Pantheon + BOSS BAO/$f\sigma_8$ + Ext-BAO + S_8, $Planck$ + Pantheon + EFTofBOSS + Ext-BAO and $Planck$ + Pantheon + EFTofBOSS + Ext-BAO + S_8 analyses for the ΛCDM model. Since we rounded the χ^2 of each experiment, the total χ^2 is only equal to the sum of each χ^2 at $\mathcal{O}(0.1)$ precision.

	ΛCDM		
Dataset	w/BAO/$f\sigma_8$ + S_8	w/EFTofBOSS	w/EFTofBOSS + S_8
$Planck$ high-l TTTEEE	2349.0	2347.4	2349.3
$Planck$ low-l EE	396.1	396.7	396.1
$Planck$ low-l TT	22.8	23.0	22.7
$Planck$ lensing	9.6	8.9	9.6
Pantheon	1027.0	1027.1	1027.0
Ext-BAO	6.3	6.2	6.3
BOSS BAO/$f\sigma_8$	6.0	⋯	⋯
EFTofBOSS	⋯	117.8	117.0
S_8	5.3	⋯	5.0
Total $\chi^2_{\min}$	3821.9	3927.0	3933.0

APPENDIX D: SUPPLEMENTARY TABLES OF $\chi^2_{\mathbf{min}}$ VALUES PER EXPERIMENT

In this Appendix, we report the best-fit χ^2 per experiment for both ΛCDM (Table VIII) and DCDM → WDM + DR (Table IX) models for our analyses with the BAO/$f\sigma_8$ + S_8, EFTofBOSS and EFTofBOSS + S_8 data. To help the reader gauge the goodness of fit, the number of d.o.f. is estimated to be 2287 for $Planck$ high-l TTTEEE, 25 for $Planck$ low-l EE, and 25 for $Planck$ low-l TT [3]. Other experiments do not report the number of degrees of freedom, but it can be estimated from the number of data points N_{data}, assuming uncorrelated data points for simplicity, and the number of free parameters $N_{\text{param}} = N_{\text{param,model}} + N_{\text{param,nuisance}}$, as $N_{\text{dof}} = N_{\text{data}} - N_{\text{param}}$. In practice, we have $N_{\text{data}} = 1048$ and $N_{\text{param,nuisance}} = 1$ for Pantheon [162], $N_{\text{data}} = 132$ and

$N_{\text{param,nuisance}} = 6$ for the sum of the three sky-cuts of the EFTofBOSS data including BAO, and $N_{\text{data}} = 13$ for the BOSS BAO/$f\sigma_8$ and Ext-BAO (the full BAO dataset). Finally, we have for each model $N_{\text{param},\Lambda\text{CDM}} = 6$ and $N_{\text{param},\Lambda\text{DCDM}} = 8$.

APPENDIX E: ΛCDM PARAMETERS OF THE DCDM → WDM + DR MODEL

In this Appendix, we compare in Fig. 16 the ΛCDM parameters of the DCDM → WDM + DR model obtained from the analyses with (blue) and without (red) the EFTofBOSS data, while in Fig. 17 we represent the ΛCDM parameters reconstructed from an analysis of $Planck$, Pantheon, Ext-BAO and EFTofBOSS data, with (blue) and without (red) the S_8 prior. We also show in this second figure the standard ΛCDM posteriors as a reference

TABLE IX. χ^2 of each dataset for our $Planck$ + Pantheon + BOSS BAO/$f\sigma_8$ + Ext-BAO + S_8, $Planck$ + Pantheon + EFTofBOSS + Ext-BAO and $Planck$ + Pantheon + EFTofBOSS + Ext-BAO + S_8 analyses for the DCDM → WDM + DR model. Since we rounded the χ^2 of each experiment, the total χ^2 is only equal to the sum of each χ^2 at $\mathcal{O}(0.1)$ precision.

	DCDM → WDM + DR		
Dataset	w/BAO/$f\sigma_8$ + S_8	w/EFTofBOSS	w/EFTofBOSS + S_8
$Planck$ high-l TTTEEE	2347.7	2347.3	2348.0
$Planck$ low-l EE	397.2	396.9	397.0
$Planck$ low-l TT	23.1	23.0	23.2
$Planck$ lensing	8.9	8.9	9.1
Pantheon	1027.2	1027.1	1027.2
Ext-BAO	6.1	6.2	6.2
BOSS BAO/$f\sigma_8$	7.1	⋯	⋯
EFTofBOSS	⋯	117.8	118.3
S_8	0.2	⋯	0.4
Total $\chi^2_{\min}$	3817.5	3927.0	3929.2

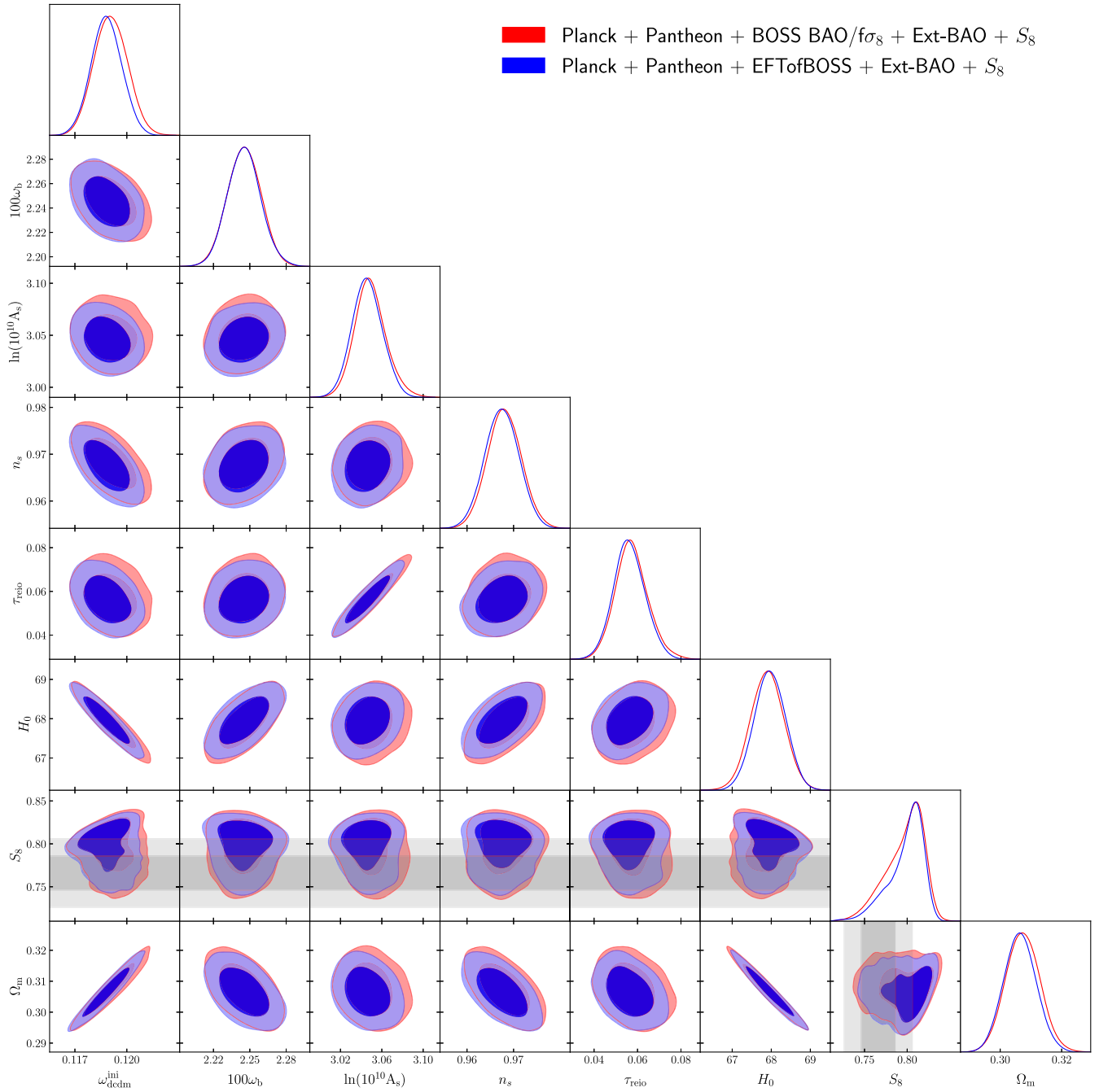FIG. 16.   2D posterior distributions of the DCDM → WDM + DR model with and without the EFTofBOSS dataset for the ΛCDM parameters. We took into account the S_8 prior from KIDS-1000 for these two MCMC analyses. The gray shaded bands refer to the joint S_8 measurement from KIDS-1000 + BOSS + 2dFLens.
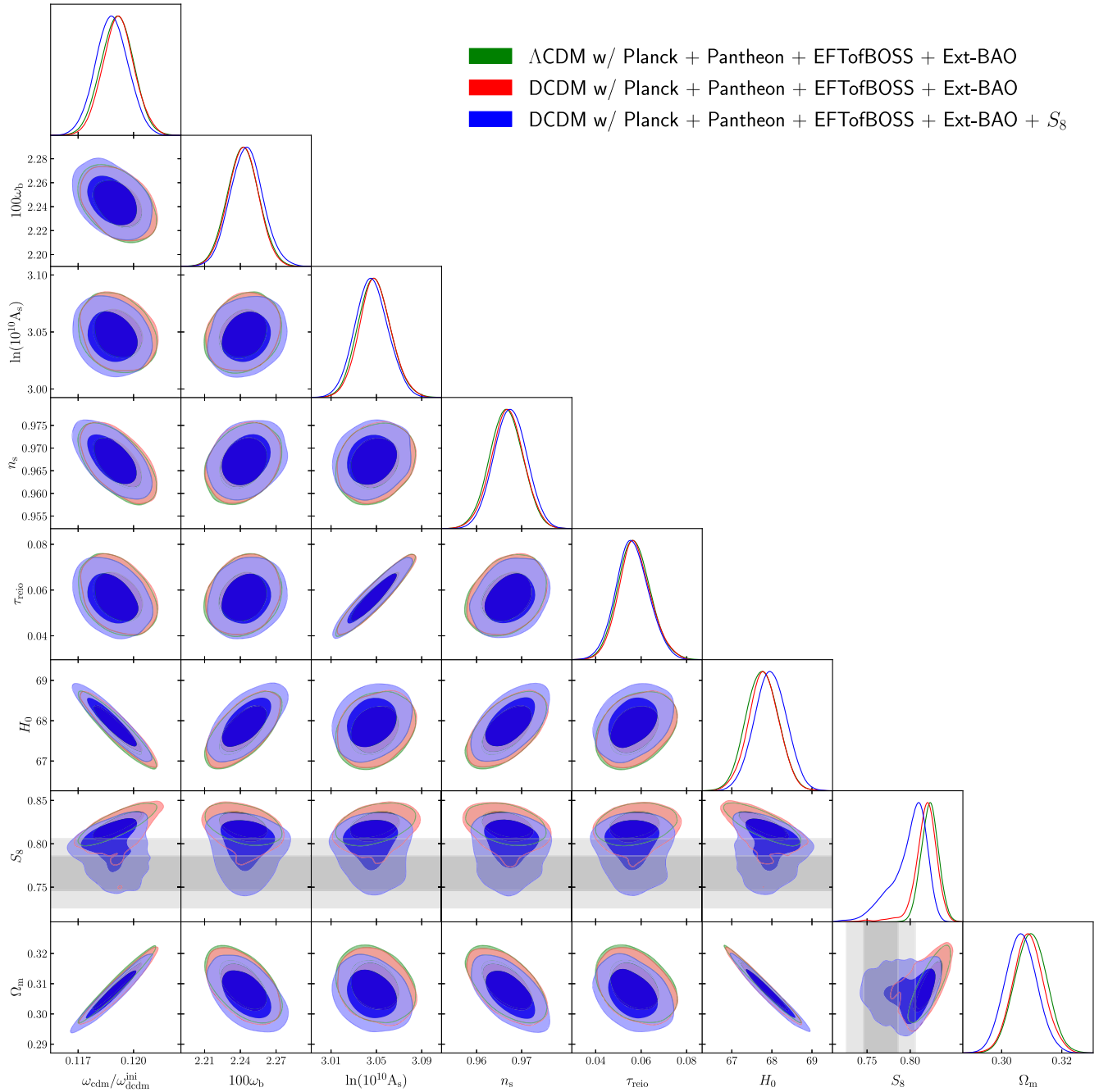
FIG. 17. 2D posterior distributions of the DCDM → WDM + DR model with and without the S_8 prior from KiDS-1000. We also plot the 2D posterior distribution for the ΛCDM model without this S_8 prior. We took into account the EFTofBOSS data for these three MCMC analyses. The gray shaded bands refer to the joint S_8 measurement from KiDS-1000 + BOSS + 2dFLens.

(green). One can see that the ΛCDM parameters are left largely unchanged in the DCDM → WDM + DR model. The decay into warm products only affects the growth of structure at late times with little impact on parameters that could affect early time physics. This is essentially why cosmological data other than those measuring S_8 (and potentially the growth of structure at late times) are unaffected by the DCDM, despite a lower S_8 value.

[1] L. Verde, T. Treu, and A. G. Riess, Tensions between the early and the late universe, Nat. Astron. **3,** 891 (2019).

[2] Adam G. Riess *et al.*, A comprehensive measurement of the local value of the Hubble constant with 1 km/s/Mpc uncertainty from the Hubble space telescope and the SH0ES team, arXiv:2112.04510.

[3] N. Aghanim *et al.* (Planck Collaboration), Planck 2018 results, Astron. Astrophys. **641,** A6 (2020).

[4] Alexie Leauthaud *et al.*, Lensing is low: Cosmology, galaxy formation, or new physics?, Mon. Not. R. Astron. Soc. **467,** 3024 (2017).

[5] Johannes U. Lange, Alexie Leauthaud, Sukhdeep Singh, Hong Guo, Rongpu Zhou, Tristan L. Smith, and Francis-Yan Cyr-Racine, On the halo-mass and radial scale dependence of the lensing is low effect, Mon. Not. R. Astron. Soc. **502,** 2074 (2021).

[6] A. Amon *et al.*, Consistent lensing and clustering in a low-S_8 Universe with BOSS, DES Year 3, HSC Year 1 and KiDS-1000, arXiv:2202.07440.

[7] Marika Asgari *et al.* (KiDS Collaboration), KiDS-1000 cosmology: Cosmic shear constraints and comparison between two point statistics, Astron. Astrophys. **645,** A104 (2021).

[8] T. M. C. Abbott *et al.* (DES Collaboration), Dark energy survey year 3 results: Cosmological constraints from galaxy clustering and weak lensing, Phys. Rev. D **105,** 023520 (2022).

[9] Chiaki Hikage *et al.* (HSC Collaboration), Cosmology from cosmic shear power spectra with Subaru Hyper Suprime-Cam first-year data, Publ. Astron. Soc. Jpn. **71,** 43 (2019).

[10] Simone Aiola *et al.* (ACT Collaboration), The Atacama Cosmology Telescope: DR4 maps and cosmological parameters, J. Cosmol. Astropart. Phys. 12 (2020) 047.

[11] Wendy L. Freedman, Measurements of the Hubble constant: Tensions in perspective, Astrophys. J. **919,** 16 (2021).

[12] Gerrit S. Farren, Oliver H. E. Philcox, and Blake D. Sherwin, Determining the Hubble constant without the sound horizon: Perspectives with future galaxy surveys, Phys. Rev. D **105,** 063503 (2022).

[13] Oliver H. E. Philcox, Gerrit S. Farren, Blake D. Sherwin, Eric J. Baxter, and Dillon J. Brout, Determining the Hubble constant without the sound horizon: A 3.6% constraint on h_0 from galaxy surveys, CMB lensing and supernovae (2022), arXiv:2204.02984.

[14] Jose Luis Bernal, Licia Verde, and Adam G. Riess, The trouble with H0, J. Cosmol. Astropart. Phys. 10 (2016) 019.

[15] Kevin Aylor, MacKenzie Joy, Lloyd Knox, Marius Millea, Srinivasan Raghunathan, and W. L. Kimmy Wu, Sounds discordant: Classical distance ladder and ΛCDM-based determinations of the cosmological sound horizon, Astrophys. J. **874,** 4 (2019).

[16] Lloyd Knox and Marius Millea, Hubble constant hunter's guide, Phys. Rev. D **101,** 043533 (2020).

[17] David Camarena and Valerio Marra, On the use of the local prior on the absolute magnitude of type ia supernovae in cosmological inference, Mon. Not. R. Astron. Soc. **504,** 5164 (2021).

[18] George Efstathiou, To H0 or not to H0?, Mon. Not. R. Astron. Soc. **505,** 3866 (2021).

[19] Nils Schöneberg, Guillermo Franco Abellán, Andrea Pérez Sánchez, Samuel J. Witte, Vivian Poulin, and Julien Lesgourgues, The H_0 olympics: A fair ranking of proposed models, arXiv:2107.10291.

[20] Christina D. Kreisch, Francis-Yan Cyr-Racine, and Olivier Doré, Neutrino puzzle: Anomalies, interactions, and cosmological tensions, Phys. Rev. D **101,** 123505 (2020).

[21] Maximilian Berbig, Sudip Jana, and Andreas Trautner, The Hubble tension and a renormalizable model of gauged neutrino self-interactions, Phys. Rev. D **102,** 115008 (2020).

[22] Subhajit Ghosh, Rishi Khatri, and Tuhin S. Roy, Can dark neutrino interactions phase out the Hubble tension?, Phys. Rev. D **102,** 123544 (2020).

[23] Francesco Forastieri, Massimiliano Lattanzi, and Paolo Natoli, Cosmological constraints on neutrino self-interactions with a light mediator, Phys. Rev. D **100,** 103526 (2019).

[24] Miguel Escudero and Samuel J. Witte, A CMB search for the neutrino mass mechanism and its relation to the Hubble tension, Eur. Phys. J. C **80,** 294 (2020).

[25] Miguel Escudero and Samuel J. Witte, The Hubble tension as a hint of leptogenesis and neutrino mass generation, Eur. Phys. J. C **81,** 515 (2021).

[26] Nikita Blinov and Gustavo Marques-Tavares, Interacting radiation after Planck and its implications for the Hubble tension, J. Cosmol. Astropart. Phys. 09 (2020) 029.

[27] Subhajit Ghosh, Soubhik Kumar, and Yuhsin Tsai, Free-streaming and coupled dark radiation isocurvature perturbations: Constraints and application to the Hubble tension, J. Cosmol. Astropart. Phys. 05 (2022) 014.

[28] Maria Archidiacono and Stefano Gariazzo, Two sides of the same coin: Sterile neutrinos and dark radiation. Status and perspectives, Universe **8,** 175 (2022).

[29] Daniel Aloni, Asher Berlin, Melissa Joseph, Martin Schmaltz, and Neal Weiner, A step in understanding the Hubble tension, Phys. Rev. D **105,** 123516 (2022).

[30] Tanvi Karwal and Marc Kamionkowski, Dark energy at early times, the Hubble parameter, and the string axiverse, Phys. Rev. D **94,** 103523 (2016).

[31] Vivian Poulin, Tristan L. Smith, Tanvi Karwal, and Marc Kamionkowski, Early Dark Energy Can Resolve the Hubble Tension, Phys. Rev. Lett. **122,** 221301 (2019).

[32] Tristan L. Smith, Vivian Poulin, and Mustafa A. Amin, Oscillating scalar fields and the Hubble tension: A resolution with novel signatures, Phys. Rev. D **101,** 063523 (2020).

[33] Florian Niedermann and Martin S. Sloth, New early dark energy, Phys. Rev. D **103,** L041303 (2021).

[34] Florian Niedermann and Martin S. Sloth, Resolving the Hubble tension with new early dark energy, Phys. Rev. D **102,** 063527 (2020).

[35] Gen Ye and Yun-Song Piao, Is the Hubble tension a hint of AdS phase around recombination?, Phys. Rev. D **101,** 083507 (2020).

[36] Janina Renk, Miguel Zumalacárregui, Francesco Montanari, and Alexandre Barreira, Galileon gravity in

light of ISW, CMB, BAO and H_0 data, J. Cosmol. Astropart. Phys. 10 (2017) 020.

[37] C. Umiltà, M. Ballardini, F. Finelli, and D. Paoletti, CMB and BAO constraints for an induced gravity dark energy model with a quartic potential, J. Cosmol. Astropart. Phys. 08 (2015) 017.

[38] Mario Ballardini, Fabio Finelli, Caterina Umiltà, and Daniela Paoletti, Cosmological constraints on induced gravity dark energy models, J. Cosmol. Astropart. Phys. 05 (2016) 067.

[39] Massimo Rossi, Mario Ballardini, Matteo Braglia, Fabio Finelli, Daniela Paoletti, Alexei A. Starobinsky, and Caterina Umiltà, Cosmological constraints on post-Newtonian parameters in effectively massless scalar-tensor theories of gravity, Phys. Rev. D **100**, 103524 (2019).

[40] Matteo Braglia, Mario Ballardini, William T. Emond, Fabio Finelli, A. Emir Gumrukcuoglu, Kazuya Koyama, and Daniela Paoletti, Larger value for H_0 by an evolving gravitational constant, Phys. Rev. D **102**, 023529 (2020).

[41] Miguel Zumalacarregui, Gravity in the era of equality: Towards solutions to the Hubble problem without fine-tuned initial conditions, Phys. Rev. D **102**, 023523 (2020).

[42] Tal Abadi and Ely D. Kovetz, Can conformally coupled modified gravity solve the Hubble tension?, Phys. Rev. D **103**, 023530 (2021).

[43] Mario Ballardini, Matteo Braglia, Fabio Finelli, Daniela Paoletti, Alexei A. Starobinsky, and Caterina Umiltà, Scalar-tensor theories of gravity, neutrino physics, and the H_0 tension, J. Cosmol. Astropart. Phys. 10 (2020) 044.

[44] Matteo Braglia, William T. Emond, Fabio Finelli, A. Emir Gumrukcuoglu, and Kazuya Koyama, Unified framework for early dark energy from α-attractors, Phys. Rev. D **102**, 083513 (2020).

[45] Eleonora Di Valentino, Alessandro Melchiorri, and Joseph Silk, Cosmological hints of modified gravity?, Phys. Rev. D **93**, 023513 (2016).

[46] Sebastian Bahamonde, Konstantinos F. Dialektopoulos, Celia Escamilla-Rivera, Gabriel Farrugia, Viktor Gakis, Martin Hendry, Manuel Hohmann, Jackson Levi Said, Jurgen Mifsud, and Eleonora Di Valentino, Teleparallel gravity: From theory to cosmology, arXiv:2106.13793.

[47] Marco Raveri, Reconstructing gravity on cosmological scales, Phys. Rev. D **101**, 083524 (2020).

[48] Sheng-Feng Yan, Pierre Zhang, Jie-Wen Chen, Xin-Zhe Zhang, Yi-Fu Cai, and Emmanuel N. Saridakis, Interpreting cosmological tensions from the effective field theory of torsional gravity, Phys. Rev. D **101**, 121301 (2020).

[49] Noemi Frusciante, Simone Peirone, Luis Atayde, and Antonio De Felice, Phenomenology of the generalized cubic covariant Galileon model and cosmological bounds, Phys. Rev. D **101**, 064001 (2020).

[50] Joan Solà Peracaula, Adria Gomez-Valent, Javier de Cruz Pérez, and Cristian Moreno-Pulido, Brans-Dicke gravity with a cosmological constant smoothes out ΛCDM tensions, Astrophys. J. Lett. **886**, L6 (2019).

[51] Joan Solà Peracaula, Adrià Gómez-Valent, Javier de Cruz Pérez, and Cristian Moreno-Pulido, Brans-Dicke cosmology with a Λ-term: A possible solution to ΛCDM tensions, Classical Quantum Gravity **37**, 245003 (2020).

[52] Guillermo Ballesteros, Alessio Notari, and Fabrizio Rompineve, The H_0 tension: ΔG_N vs $\Delta N_{\rm eff}$, J. Cosmol. Astropart. Phys. 11 (2020) 024.

[53] Matteo Braglia, Mario Ballardini, Fabio Finelli, and Kazuya Koyama, Early modified gravity in light of the H_0 tension and LSS data, Phys. Rev. D **103**, 043528 (2021).

[54] Harry Desmond, Bhuvnesh Jain, and Jeremy Sakstein, Local resolution of the Hubble tension: The impact of screened fifth forces on the cosmic distance ladder, Phys. Rev. D **100**, 043537 (2019).

[55] Meng-Xiang Lin, Marco Raveri, and Wayne Hu, Phenomenology of modified gravity at recombination, Phys. Rev. D **99**, 043514 (2019).

[56] Chi-Ting Chiang and Anže Slosar, Inferences of H_0 in presence of a non-standard recombination, arXiv:1811.03624.

[57] Luke Hart and Jens Chluba, Updated fundamental constant constraints from Planck 2018 data and possible relations to the Hubble tension, Mon. Not. R. Astron. Soc. **493**, 3255 (2020).

[58] Toyokazu Sekiguchi and Tomo Takahashi, Early recombination as a solution to the H_0 tension, Phys. Rev. D **103**, 083507 (2021).

[59] Karsten Jedamzik and Levon Pogosian, Relieving the Hubble Tension with Primordial Magnetic Fields, Phys. Rev. Lett. **125**, 181302 (2020).

[60] Francis-Yan Cyr-Racine, Fei Ge, and Lloyd Knox, A Symmetry of Cosmological Observables, and a High Hubble Constant as an Indicator of a Mirror World Dark Sector, Phys. Rev. Lett. **128**, 201301 (2022).

[61] Eleonora Di Valentino, Olga Mena, Supriya Pan, Luca Visinelli, Weiqiang Yang, Alessandro Melchiorri, David F. Mota, Adam G. Riess, and Joseph Silk, In the realm of the Hubble tension—A review of solutions, Classical Quantum Gravity **38**, 153001 (2021).

[62] Julien Lesgourgues, Gustavo Marques-Tavares, and Martin Schmaltz, Evidence for dark matter interactions in cosmological precision data?, J. Cosmol. Astropart. Phys. 02 (2016) 037.

[63] Manuel A. Buen-Abad, Gustavo Marques-Tavares, and Martin Schmaltz, Non-Abelian dark matter and dark radiation, Phys. Rev. D **92**, 023531 (2015).

[64] Zackaria Chacko, Yanou Cui, Sungwoo Hong, Takemichi Okui, and Yuhsin Tsai, Partially acoustic dark matter, interacting dark radiation, and large scale structure, J. High Energy Phys. 12 (2016) 108.

[65] Manuel A. Buen-Abad, Martin Schmaltz, Julien Lesgourgues, and Thejs Brinckmann, Interacting dark sector and precision cosmology, J. Cosmol. Astropart. Phys. 01 (2018) 008.

[66] Stefan Heimersheim, Nils Schöneberg, Deanna C. Hooper, and Julien Lesgourgues, Cannibalism hinders growth: Cannibal dark matter and the S_8 tension, J. Cosmol. Astropart. Phys. 12 (2020) 016.

[67] Adrià Gómez-Valent, Valeria Pettorino, and Luca Amendola, Update on coupled dark energy and the H_0 tension, Phys. Rev. D **101**, 123513 (2020).

[68] Eleonora Di Valentino, Alessandro Melchiorri, Olga Mena, and Sunny Vagnozzi, Interacting dark energy in the early

2020s: A promising solution to the H_0 and cosmic shear tensions, Phys. Dark Universe **30,** 100666 (2020).

[69] Matteo Lucca, Dark energy–dark matter interactions as a solution to the S8 tension, Phys. Dark Universe **34,** 100899 (2021).

[70] Guillermo F. Abellan, Riccardo Murgia, Vivian Poulin, and Julien Lavalle, Hints for decaying dark matter from S_8 measurements, Phys. Rev. D **105,** 063525 (2022).

[71] Eleonora Di Valentino *et al.*, Cosmology intertwined III: $f\sigma_8$ and S_8, Astropart. Phys. **131,** 102604 (2021).

[72] Saurabh Bansal, Jeong Han Kim, Christopher Kolda, Matthew Low, and Yuhsin Tsai, Mirror twin Higgs cosmology: Constraints and a possible resolution to the H_0 and S_8 tensions, J. High Energy Phys. 05 (2022) 050.

[73] Kari Enqvist, Seshadri Nadathur, Toyokazu Sekiguchi, and Tomo Takahashi, Decaying dark matter and the tension in σ_8, J. Cosmol. Astropart. Phys. 09 (2015) 067.

[74] Z. Berezhiani, A. D. Dolgov, and I. I. Tkachev, Reconciling Planck results with low redshift astronomical measurements, Phys. Rev. D **92,** 061303 (2015).

[75] Nikita Blinov, Celeste Keith, and Dan Hooper, Warm decaying dark matter and the Hubble tension, J. Cosmol. Astropart. Phys. 06 (2020) 005.

[76] Kyriakos Vattis, Savvas M. Koushiappas, and Abraham Loeb, Late universe decaying dark matter can relieve the H_0 tension, Phys. Rev. D **99,** 121302 (2019).

[77] Guillermo F. Abellán, Riccardo Murgia, and Vivian Poulin, Linear cosmological constraints on 2-body decaying dark matter scenarios and robustness of the resolution to the S_8 tension, Phys. Rev. D **104,** 123533 (2021).

[78] A. Chudaykin, D. Gorbunov, and I. Tkachev, Dark matter component decaying after recombination: Lensing constraints with Planck data, Phys. Rev. D **94,** 023528 (2016).

[79] A. Chudaykin, D. Gorbunov, and I. Tkachev, Dark matter component decaying after recombination: Sensitivity to baryon acoustic oscillation and redshift space distortion probes, Phys. Rev. D **97,** 083508 (2018).

[80] Vivian Poulin, Pasquale D. Serpico, and Julien Lesgourgues, A fresh look at linear cosmological constraints on a decaying dark matter component, J. Cosmol. Astropart. Phys. 08 (2016) 036.

[81] Steven J. Clark, Kyriakos Vattis, and Savvas M. Koushiappas, Cosmological constraints on late-Universe decaying dark matter as a solution to the H0 tension, Phys. Rev. D **103,** 043014 (2021).

[82] Balakrishna S. Haridasu and Matteo Viel, Late-time decaying dark matter: Constraints and implications for the H0-tension, Mon. Not. R. Astron. Soc. **497,** 1757 (2020).

[83] Andreas Nygaard, Thomas Tram, and Steen Hannestad, Updated constraints on decaying cold dark matter, J. Cosmol. Astropart. Phys. 05 (2021) 017.

[84] S. Alvi, T. Brinckmann, M. Gerbino, M. Lattanzi, and L. Pagano, Do you smell something decaying? Updated linear constraints on decaying dark matter scenarios, arXiv:2205.05636.

[85] V. Berezinsky, A. Masiero, and J. W. F. Valle, Cosmological signatures of supersymmetry with spontaneously broken R parity, Phys. Lett. B **266,** 382 (1991).

[86] Hang Bae Kim and Jihn E. Kim, Late decaying axino as CDM and its lifetime bound, Phys. Lett. B **527,** 18 (2002).

[87] Laura Covi, Jihn E. Kim, and Leszek Roszkowski, Axinos as Cold Dark Matter, Phys. Rev. Lett. **82,** 4180 (1999).

[88] J. L. Feng, A. Rajaraman, and F. Takayama, Superweakly Interacting Massive Particles, Phys. Rev. Lett. **91,** 011302 (2003).

[89] Jonathan L. Feng, Arvind Rajaraman, and Fumihiro Takayama, Superweakly interacting massive particle dark matter signals from the early universe, Phys. Rev. D **68,** 063504 (2003).

[90] Rouzbeh Allahverdi, Bhaskar Dutta, Farinaldo S. Queiroz, Louis E. Strigari, and Mei-Yu Wang, Dark matter from late invisible decays to and of gravitinos, Phys. Rev. D **91,** 055033 (2015).

[91] K. N. Abazajian *et al.*, Light sterile neutrinos: A white paper, arXiv:1204.5379.

[92] M. Drewes *et al.*, A white paper on keV sterile neutrino dark matter, J. Cosmol. Astropart. Phys. 01 (2017) 025.

[93] Chuan-Ren Chen, Fuminobu Takahashi, and T. T. Yanagida, Gamma rays and positrons from a decaying hidden gauge boson, Phys. Lett. B **671,** 71 (2009).

[94] Gongjun Choi, Motoo Suzuki, and Tsutomu T. Yanagida, Degenerate sub-keV fermion dark matter from a solution to the Hubble tension, Phys. Rev. D **101,** 075031 (2020).

[95] Gongjun Choi, Motoo Suzuki, and Tsutomu T. Yanagida, Degenerate fermion dark matter from a broken U(1)B-L gauge symmetry, Phys. Rev. D **102,** 035022 (2020).

[96] Gongjun Choi and Tsutomu T. Yanagida, Gravitino cosmology helped by a right handed (s)neutrino, Phys. Lett. B **827,** 136954 (2022).

[97] Emil Brinch Holm, Thomas Tram, and Steen Hannestad, Decaying warm dark matter revisited, arXiv:2205.13628.

[98] Gongjun Choi, Motoo Suzuki, and Tsutomu T. Yanagida, XENON1T anomaly and its implication for decaying warm dark matter, Phys. Lett. B **811,** 135976 (2020).

[99] Shuai Xu and Sibo Zheng, Resolving xenon excess with decaying cold dark matter, Eur. Phys. J. C **81,** 446 (2021).

[100] Koushik Dutta, Avirup Ghosh, Arpan Kar, and Biswarup Mukhopadhyaya, Decaying fermionic warm dark matter and XENON1T electronic recoil excess, Phys. Dark Universe **33,** 100855 (2021).

[101] W. B. Lin, D. H. Huang, X. Zhang, and R. Brandenberger, Nonthermal Production of Weakly Interacting Massive Particles and the Subgalactic Structure of the Universe, Phys. Rev. Lett. **86,** 954 (2001).

[102] F. J. Sánchez-Salcedo, Unstable cold dark matter and the cuspy halo problem in dwarf galaxies, Astrophys. J. **591,** L107 (2003).

[103] J. A. R. Cembranos, J. L. Feng, A. Rajaraman, and F. Takayama, Superweakly Interacting Massive Particle Solutions to Small Scale Structure Problems, Phys. Rev. Lett. **95,** 181301 (2005).

[104] Manoj Kaplinghat, Dark matter from early decays, Phys. Rev. D **72,** 063510 (2005).

[105] Louis E. Strigari, Manoj Kaplinghat, and James S. Bullock, Dark matter halos with cores from hierarchical structure formation, Phys. Rev. D **75,** 061303 (2007).

[106] F. Borzumati, T. Bringmann, and P. Ullio, Dark matter from late decays and the small-scale structure problems, Phys. Rev. D **77,** 063514 (2008).

[107] Annika H. G. Peter, Christopher E. Moody, and Marc Kamionkowski, Dark-matter decays and self-gravitating halos, Phys. Rev. D **81,** 103501 (2010).

[108] Annika H. G. Peter and Andrew J. Benson, Dark-matter decays and Milky Way satellite galaxies, Phys. Rev. D **82,** 123521 (2010).

[109] John Joseph M. Carrasco, Mark P. Hertzberg, and Leonardo Senatore, The effective field theory of cosmological large scale structures, J. High Energy Phys. 09 (2012) 082.

[110] Daniel Baumann, Alberto Nicolis, Leonardo Senatore, and Matias Zaldarriaga, Cosmological non-linearities as an effective fluid, J. Cosmol. Astropart. Phys. 07 (2012) 051.

[111] Rafael A. Porto, Leonardo Senatore, and Matias Zaldarriaga, The Lagrangian-space effective field theory of large scale structures, J. Cosmol. Astropart. Phys. 05 (2014) 022.

[112] Enrico Pajer and Matias Zaldarriaga, On the renormalization of the effective field theory of large scale structures, J. Cosmol. Astropart. Phys. 08 (2013) 037.

[113] Ali Akbar Abolhasani, Mehrdad Mirbabayi, and Enrico Pajer, Systematic renormalization of the effective theory of large scale structure, J. Cosmol. Astropart. Phys. 05 (2016) 063.

[114] Leonardo Senatore and Matias Zaldarriaga, Redshift space distortions in the effective field theory of large scale structures, arXiv:1409.1225.

[115] Tobias Baldauf, Mehrdad Mirbabayi, Marko Simonovic, and Matias Zaldarriaga, Equivalence principle and the baryon acoustic peak, Phys. Rev. D **92,** 043514 (2015).

[116] Leonardo Senatore and Matias Zaldarriaga, The IR-resummed effective field theory of large scale structures, J. Cosmol. Astropart. Phys. 02 (2015) 013.

[117] Leonardo Senatore and Gabriele Trevisan, On the IR-resummation in the EFTofLSS, J. Cosmol. Astropart. Phys. 05 (2018) 019.

[118] Matthew Lewandowski and Leonardo Senatore, An analytic implementation of the IR-resummation for the BAO peak, J. Cosmol. Astropart. Phys. 03 (2020) 018.

[119] Diego Blas, Mathias Garny, Mikhail M. Ivanov, and Sergey Sibiryakov, Time-sliced perturbation theory II: Baryon acoustic oscillations and infrared resummation, J. Cosmol. Astropart. Phys. 07 (2016) 028.

[120] John Joseph M. Carrasco, Simon Foreman, Daniel Green, and Leonardo Senatore, The 2-loop matter power spectrum and the IR-safe integrand, volume = 2014, J. Cosmol. Astropart. Phys. 07 (2014) 056.

[121] John Joseph M. Carrasco, Simon Foreman, Daniel Green, and Leonardo Senatore, The effective field theory of large scale structures at two loops, J. Cosmol. Astropart. Phys. 07 (2014) 057.

[122] Leonardo Senatore, Bias in the effective field theory of large scale structures, J. Cosmol. Astropart. Phys. 11 (2015) 007.

[123] Mehrdad Mirbabayi, Fabian Schmidt, and Matias Zaldarriaga, Biased tracers and time evolution, J. Cosmol. Astropart. Phys. 07 (2015) 030.

[124] Raul Angulo, Matteo Fasiello, Leonardo Senatore, and Zvonimir Vlah, On the statistics of biased tracers in the effective field theory of large scale structures, J. Cosmol. Astropart. Phys. 09 (2015) 029.

[125] Tomohiro Fujita, Valentin Mauerhofer, Leonardo Senatore, Zvonimir Vlah, and Raul Angulo, Very massive tracers and higher derivative biases, J. Cosmol. Astropart. Phys. 01 (2020) 009.

[126] Ashley Perko, Leonardo Senatore, Elise Jennings, and Risa H. Wechsler, Biased tracers in redshift space in the EFT of large-scale structure, arXiv:1610.09321.

[127] Ethan O. Nadler, Ashley Perko, and Leonardo Senatore, On the bispectra of very massive tracers in the effective field theory of large-scale structure, J. Cosmol. Astropart. Phys. 02 (2018) 058.

[128] Guido D'Amico, Leonardo Senatore, and Pierre Zhang, Limits on wCDM from the EFTofLSS with the PyBird code, J. Cosmol. Astropart. Phys. 01 (2021) 006.

[129] C. Alcock and B. Paczynski, An evolution free test for non-zero cosmological constant, Nature (London) **281,** 358 (1979).

[130] Florian Beutler, Emanuele Castorina, and Pierre Zhang, Interpreting measurements of the anisotropic galaxy power spectrum, J. Cosmol. Astropart. Phys. 03 (2019) 040.

[131] ChangHoon Hahn, Roman Scoccimarro, Michael R. Blanton, Jeremy L. Tinker, and Sergio Rodríguez-Torres, The effect of fiber collisions on the galaxy power spectrum multipoles, Mon. Not. R. Astron. Soc. **467,** 1940 (2017).

[132] Diego Blas, Julien Lesgourgues, and Thomas Tram, The Cosmic Linear Anisotropy Solving System (CLASS). Part II: Approximation schemes, J. Cosmol. Astropart. Phys. 07 (2011) 034.

[133] Antony Lewis, Anthony Challinor, and Anthony Lasenby, Efficient computation of CMB anisotropies in closed FRW models, Astrophys. J. **538,** 473 (2000).

[134] Anton Chudaykin, Mikhail M. Ivanov, Oliver H. E. Philcox, and Marko Simonovic, Nonlinear perturbation theory extension of the Boltzmann code CLASS, Phys. Rev. D **102,** 063533 (2020).

[135] A. J. S. Hamilton, Uncorrelated modes of the nonlinear power spectrum, Mon. Not. R. Astron. Soc. **312,** 257 (2000).

[136] Marko Simonovic, Tobias Baldauf, Matias Zaldarriaga, John Joseph Carrasco, and Juna A. Kollmeier, Cosmological perturbation theory using the FFTLog: Formalism and connection to QFT loop integrals, J. Cosmol. Astropart. Phys. 04 (2018) 030.

[137] Luca Amendola et al., Cosmology and fundamental physics with the Euclid satellite, Living Rev. Relativity **21,** 2 (2018). 1606.00180.

[138] David Alonso et al. (LSST Dark Energy Science Collaboration), The LSST Dark Energy Science Collaboration (DESC) science requirements document, arXiv:1809.01669.

[139] Shadab Alam et al. (BOSS Collaboration), The clustering of galaxies in the completed SDSS-III Baryon Oscillation Spectroscopic Survey: Cosmological analysis of the DR12 galaxy sample, Mon. Not. R. Astron. Soc. **470,** 2617 (2017).

[140] Beth Reid et al., SDSS-III baryon oscillation spectroscopic survey data release 12: Galaxy target selection and large scale structure catalogues, Mon. Not. R. Astron. Soc. **455,** 1553 (2016).

[141] Francisco-Shu Kitaura *et al.*, The clustering of galaxies in the SDSS-III Baryon Oscillation Spectroscopic Survey: Mock galaxy catalogues for the BOSS Final Data Release, Mon. Not. R. Astron. Soc. **456**, 4156 (2016).

[142] Pierre Zhang, Guido D'Amico, Leonardo Senatore, Cheng Zhao, and Yifu Cai, BOSS correlation function analysis from the effective field theory of large-scale structure, J. Cosmol. Astropart. Phys. 02 (2022) 036.

[143] Guido d' Amico, Jérôme Gleyzes, Nickolas Kokron, Katarina Markovic, Leonardo Senatore, Pierre Zhang, Florian Beutler, and Héctor Gil-Marín, The cosmological analysis of the SDSS/BOSS data from the effective theory of large-scale structure, J. Cosmol. Astropart. Phys. 05 (2020) 005.

[144] Thomas Colas, Guido d' Amico, Leonardo Senatore, Pierre Zhang, and Florian Beutler, Efficient cosmological analysis of the SDSS/BOSS data from the effective field theory of large-scale structure, J. Cosmol. Astropart. Phys. 06 (2020) 001.

[145] Takahiro Nishimichi, Guido D'Amico, Mikhail M. Ivanov, Leonardo Senatore, Marko Simonovic, Masahiro Takada, Matias Zaldarriaga, and Pierre Zhang, Blinded challenge for precision cosmology with large-scale structure: Results from effective field theory for the redshift-space galaxy power spectrum, Phys. Rev. D **102**, 123541 (2020).

[146] Guido D'Amico, Leonardo Senatore, and Pierre Zhang, Limits on wCDM from the EFTofLSS with the PyBird code, J. Cosmol. Astropart. Phys. 01 (2021) 006.

[147] Benjamin Audren, Julien Lesgourgues, Gianpiero Mangano, Pasquale Dario Serpico, and Thomas Tram, Strongest model-independent bound on the lifetime of dark matter, J. Cosmol. Astropart. Phys. 12 (2014) 028.

[148] Kari Enqvist, Seshadri Nadathur, Toyokazu Sekiguchi, and Tomo Takahashi, Decaying dark matter and the tension in $\sigma 8$, J. Cosmol. Astropart. Phys. 09 (2015) 067.

[149] Chung-Pei Ma and Edmund Bertschinger, Cosmological perturbation theory in the synchronous and conformal Newtonian gauges, Astrophys. J. **455**, 7 (1995).

[150] Julien Lesgourgues and Thomas Tram, Fast and accurate CMB computations in non-flat FLRW universes, J. Cosmol. Astropart. Phys. 09 (2014) 032.

[151] Jonathan Hubert, Aurel Schneider, Doug Potter, Joachim Stadel, and Sambit K. Giri, Decaying dark matter: Simulations and weak-lensing forecast, J. Cosmol. Astropart. Phys. 10 (2021) 040.

[152] Julien Lesgourgues, Gianpiero Mangano, Gennaro Miele, and Sergio Pastor, *Neutrino Cosmology* (Cambridge University Press, Cambridge, England, 2013).

[153] Gordon Blackadder and Savvas M. Koushiappas, Dark matter with two- and many-body decays and supernovae type Ia, Phys. Rev. D **90**, 103527 (2014).

[154] Shohei Aoyama, Toyokazu Sekiguchi, Kiyotomo Ichiki, and Naoshi Sugiyama, Evolution of perturbations and cosmological constraints in decaying dark matter models with arbitrary decay mass products, J. Cosmol. Astropart. Phys. 07 (2014) 021.

[155] Julien Lesgourgues and Thomas Tram, The Cosmic Linear Anisotropy Solving System (CLASS) IV: Efficient implementation of non-cold relics, J. Cosmol. Astropart. Phys. 09 (2011) 032.

[156] Leonardo Senatore and Matias Zaldarriaga, The effective field theory of large-scale structure in the presence of massive neutrinos, arXiv:1707.04698.

[157] Roger de Belsunce and Leonardo Senatore, Tree-level bispectrum in the effective field theory of large-scale structure extended to massive neutrinos, J. Cosmol. Astropart. Phys. 02 (2019) 038.

[158] Catherine Heymans *et al.*, Kids-1000 cosmology: Multi-probe weak gravitational lensing and spectroscopic galaxy clustering constraints, Astron. Astrophys. **646**, A140 (2021).

[159] Thejs Brinckmann and Julien Lesgourgues, MONTEPY-THON3: Boosted MCMC sampler and other features, Phys. Dark Universe **24**, 100260 (2019).

[160] Benjamin Audren, Julien Lesgourgues, Karim Benabed, and Simon Prunet, Conservative constraints on early cosmology: An illustration of the Monte Python cosmological parameter inference code, J. Cosmol. Astropart. Phys. 02 (2013) 001.

[161] N. Aghanim *et al.* (Planck Collaboration), Planck 2018 results. VIII. Gravitational lensing, Astron. Astrophys. **641**, A8 (2020).

[162] D. M. Scolnic *et al.*, The complete light-curve sample of spectroscopically confirmed SNe Ia from pan-STARRS1 and cosmological constraints from the combined pantheon sample, Astrophys. J. **859**, 101 (2018).

[163] Florian Beutler, Chris Blake, Matthew Colless, D. Heath Jones, Lister Staveley-Smith, Lachlan Campbell, Quentin Parker, Will Saunders, and Fred Watson, The 6dF Galaxy Survey: Baryon acoustic oscillations and the local Hubble constant, Mon. Not. R. Astron. Soc. **416**, 3017 (2011).

[164] Ashley J. Ross, Lado Samushia, Cullan Howlett, Will J. Percival, Angela Burden, and Marc Manera, The clustering of the SDSS DR7 main Galaxy sample I: A 4 per cent distance measure at $z = 0.15$, Mon. Not. R. Astron. Soc. **449**, 835 (2015).

[165] Victoria de Sainte Agathe *et al.*, Baryon acoustic oscillations at $z = 2.34$ from the correlations of Lyα absorption in eBOSS DR14, Astron. Astrophys. **629**, A85 (2019).

[166] Michael Blomqvist *et al.*, Baryon acoustic oscillations from the cross-correlation of Lyα absorption and quasars in eBOSS DR14, Astron. Astrophys. **629**, A86 (2019).

[167] Andrew Gelman and Donald B. Rubin, Inference from iterative simulation using multiple sequences, Stat. Sci. **7**, 457 (1992).

[168] Vivian Poulin, Kimberly K. Boddy, Simeon Bird, and Marc Kamionkowski, Implications of an extended dark energy cosmology with massive neutrinos for cosmological tensions, Phys. Rev. D **97**, 123504 (2018).

[169] Marco Raveri and Wayne Hu, Concordance and discordance in cosmology, Phys. Rev. D **99**, 043506 (2019).

[170] S. Mau *et al.*, Milky Way satellite census. IV. Constraints on decaying dark matter from observations of Milky Way satellite galaxies, Astrophys. J. **932**, 128 (2022).

[171] Amir Aghamousa *et al.* (DESI Collaboration), The DESI experiment part I: Science, targeting, and survey design, arXiv:1611.00036.

[172] Catherine Heymans *et al.*, CFHTLenS tomographic weak lensing cosmological parameter constraints: Mitigating the impact of intrinsic galaxy alignments, Mon. Not. R. Astron. Soc. **432**, 2433 (2013).